INSTITUTE OF PHYSICS PUBLISHING INVERSE PROBLEMS

Inverse Problems **19** (2003) 1159–1184 PII: S0266-5611(03)57791-7

Variationally constrained numerical solution of electrical impedance tomography

Liliana Borcea[1], **Genetha Anne Gray**[2] **and Yin Zhang**[1]

[1] Computational and Applied Mathematics, MS 134, Rice University, 6100 Main Street, Houston, TX 77005-1892, USA
[2] Sandia National Laboratories, PO Box 969, MS 9217, Livermore, CA 94551-0969, USA

E-mail: borcea@caam.rice.edu, gagray@sandia.gov and zhang@caam.rice.edu

Received 18 December 2002, in final form 18 July 2003
Published 15 September 2003
Online at stacks.iop.org/IP/19/1159

Abstract

We propose a novel, variational inversion methodology for the electrical impedance tomography (EIT) problem, where we seek electrical conductivity σ inside a bounded, simply connected domain Ω, given simultaneous measurements of electric currents I and corresponding potentials V at the boundary. Explicitly, we make use of natural, variational constraints on the space of admissible functions σ, to obtain efficient reconstruction methods which make best use of the data. We give a detailed analysis of the variational constraints; we propose a variety of reconstruction algorithms for the static problem in a simple continuum model. We discuss their advantages and disadvantages and we assess the performance of our algorithms through numerical simulations and comparisons with other, well established, numerical reconstruction methods.

(Some figures in this article are in colour only in the electronic version)

1. Introduction

Electrical properties such as the electrical conductivity σ and the electric permittivity ϵ determine the behaviour of materials under the influence of external electric fields [63]. Let us consider a bounded, simply connected set $\Omega \subset \mathbb{R}^d$, for $d \geqslant 2$, and, at frequency ω, let γ be the complex admittivity function

$$\gamma(\mathbf{x}, \omega) = \sigma(\mathbf{x}) + \mathrm{i}\omega\epsilon(\mathbf{x}), \qquad \text{where } \mathrm{i} = \sqrt{-1}. \tag{1.1}$$

The electrical impedance is the reciprocal of γ and it measures the ratio between the electric field and the electric current at location $\mathbf{x} \in \Omega$. Electrical impedance tomography (EIT) is the inverse problem of determining the impedance in the interior of Ω, given simultaneous measurements of direct or alternating electric currents and voltages at the boundary $\partial\Omega$ (i.e. the Neumann-to-Dirichlet (NtD) or Dirichlet-to-Neumann (DtN) map).

Different materials display different electrical properties (see for example [11, 69, 92]), so a map of $\sigma(\mathbf{x})$ and $\epsilon(\mathbf{x})$, for $\mathbf{x} \in \Omega$, can be used to infer the internal structure in Ω. Due to this fact, EIT is an imaging tool with important applications in fields such as medicine, geophysics, environmental sciences and nondestructive testing of materials. Examples of medical applications of EIT are the detection of pulmonary emboli [26, 52, 54], monitoring of apnoea [3], monitoring of heart function and blood flow [44, 60] and breast cancer detection [26]. In geophysics and environmental sciences, EIT can be useful for locating underground mineral deposits [85], detection of leaks in underground storage tanks [87] and monitoring flows of injected fluids into the earth, for the purpose of oil extraction or environmental cleaning [88]. Finally, in nondestructive testing, EIT can be used for the detection of corrosion [89] and of small defects, such as cracks or voids, in metals [4, 5, 24, 37, 45, 91].

EIT has been studied extensively in the last two decades and substantial progress has been made in the theoretical [1, 6, 12, 17, 19, 23, 35, 42, 62, 72, 73, 76, 79, 81, 82, 84, 97, 102], numerical [18, 19, 21, 22, 26, 31, 33, 39, 49, 56–59, 66, 68, 70, 90, 95, 99, 106] and experimental [10, 26, 54, 75, 87, 96] aspects of the problem. Nevertheless, EIT remains an area of active research which continues to pose a variety of challenging questions to theoreticians, numerical analysts and experimentalists alike [19, 26, 54, 102].

In this paper, we begin by considering direct electric current excitations (i.e., $\omega = 0$), and we seek to image the electrical conductivity function $\sigma(\mathbf{x})$ inside Ω. We propose a new reconstruction methodology for EIT, based on two, dual to each other, variational principles for the NtD and DtN maps, respectively. A variational, 'equation-error' inversion method, based on the algorithm of Wexler *et al* [105], has already been analysed by Kohn and Vogelius [73] and implemented by Kohn and McKenney [70], where the electric current, the potential and the conductivity inside Ω are sought as minimizers of a functional which ensures that, at the 'solution', Ohm's law is satisfied, at least for noiseless data. We consider here a different formulation which uses the variational principles as constraints on the set of admissible conductivity functions σ. Variational constraints have been proposed by Berryman and Kohn in [13] (see also [15, 16]). However, they have only been partially analysed and their role in inversion has not been entirely understood[3]. We give a detailed analysis of the variational constraints and we show how they can be used effectively in the numerical solution of the EIT problem. We propose a variety of reconstruction algorithms and we discuss some of their advantages and disadvantages. All these algorithms guarantee that, at least in the noiseless case, Ohm's law is satisfied inside Ω and, consequently, the measured boundary potential V is fitted in the natural, $H^{\frac{1}{2}}(\partial\Omega)$ norm. In theory, our numerical algorithms achieve the same objective as the variational method considered in [70, 73]. However, due to the ill-posedness of the EIT problem, we note that, for noisy data, their numerical performance can be different. We point out the potential benefits of variationally constrained reconstructions over widely used imaging methods such as output least squares [19, 26, 106], where data are fitted in the weaker, $L^2(\partial\Omega)$ norm, at the expense of loss in resolution of the images of σ. Finally, we note that use of variational constraints is not limited to the static case and can be extended to the complex EIT problem.

This paper is organized as follows: in sections 2.1 and 2.2, we define the forward and inverse problem and we state the variational principles for the NtD and DtN maps. The variational constraints on σ, as defined originally by Berryman and Kohn [13], are given in section 2.3. In section 3, we motivate the use of variational constraints in the reconstruction

[3] There exists a variationally constrained numerical algorithm for the travel time tomography problem, due to Berryman [14]. However, this problem is considerably different from EIT, especially because Fermat's principle is not a minimum variational principle and, as such, it does not have a dual.

algorithms. A detailed analysis of the variational constraints is given in section 4. Based on this analysis, we propose a variety of reconstruction algorithms, in section 5.1. After a brief discussion of these algorithms, we concentrate on the constrained least squares formulation, which is implemented as discussed in 5.2. Some representative numerical results and comparisons with traditional least squares and the variational algorithm in [70, 73] are given in section 6. Finally, in section 7, we give a summary of the paper and conclusions.

2. The mathematical model

2.1. The forward model

We assume throughout the paper that the medium is isotropic. The electric potential $\phi(\mathbf{x})$ is defined in terms of the electric field $\mathbf{E}(\mathbf{x})$ as

$$\mathbf{E}(\mathbf{x}) = -\nabla\phi(\mathbf{x}) \tag{2.1}$$

and the current density $\mathbf{j}(\mathbf{x})$ satisfies Ohm's law

$$\mathbf{j}(\mathbf{x}) = -\sigma(\mathbf{x})\nabla\phi(\mathbf{x}), \tag{2.2}$$

where $\sigma(\mathbf{x})$ is a scalar valued, bounded, and strictly positive measurable function in $\bar{\Omega}$, the closure of the domain. When there are no sources of current inside Ω, $\mathbf{j}$ satisfies

$$\nabla \cdot [\sigma(\mathbf{x})\nabla\phi(\mathbf{x})] = 0 \qquad \text{in } \Omega, \tag{2.3}$$

which we take with either Dirichlet boundary conditions

$$\phi(\mathbf{x}) = V(\mathbf{x}), \qquad \text{for } \mathbf{x} \in \partial\Omega, \tag{2.4}$$

or Neumann boundary conditions

$$\sigma(\mathbf{x})\nabla\phi(\mathbf{x}) \cdot \mathbf{n}(\mathbf{x}) \equiv \sigma(\mathbf{x})\frac{\partial\phi(\mathbf{x})}{\partial n} = I(\mathbf{x}) \qquad \text{at } \partial\Omega, \text{ such that } \int_{\partial\Omega} I(\mathbf{x})\,\mathrm{d}s(\mathbf{x}) = 0, \tag{2.5}$$

where $\mathbf{n}(\mathbf{x})$ is the outer normal at $\mathbf{x} \in \partial\Omega$. It is well known that Dirichlet boundary value problem (2.3), (2.4), for arbitrary $V \in H^{\frac{1}{2}}(\partial\Omega)$, has a unique solution $\phi(\mathbf{x}) \in H^1(\Omega)$, at least in the weak sense [43]. Neumann boundary value problem (2.3), (2.5), for $I \in H^{-\frac{1}{2}}(\partial\Omega)$, has a unique solution $\phi(\mathbf{x}) \in H^1(\Omega)$, up to an additive constant [43], which we fix by choosing the ground as

$$\int_{\partial\Omega} \phi(\mathbf{x})\,\mathrm{d}s(\mathbf{x}) = \int_{\partial\Omega} V(\mathbf{x})\,\mathrm{d}s(\mathbf{x}) = 0. \tag{2.6}$$

The electric current density satisfies equations

$$\begin{aligned} &\nabla \times \left[\frac{1}{\sigma(\mathbf{x})}\mathbf{j}(\mathbf{x})\right] = 0 \qquad \text{and} \qquad \nabla \cdot \mathbf{j}(\mathbf{x}) = 0 \qquad \text{in } \Omega, \\ &-\mathbf{j}(\mathbf{x}) \cdot \mathbf{n}(\mathbf{x}) = I(\mathbf{x}), \qquad \text{for } \mathbf{x} \in \partial\Omega, \text{ such that } \int_{\partial\Omega} I(\mathbf{x})\,\mathrm{d}s(\mathbf{x}) = 0, \end{aligned} \tag{2.7}$$

which, by (2.2), are equivalent to (2.3), (2.5). In particular, we have that (2.7) has a unique solution $\mathbf{j}(\mathbf{x})$, with bounded norm in $L^2(\Omega)$, which is related to potential $\phi(\mathbf{x}) \in H^1(\Omega)$, a solution of (2.3), (2.5), by Ohm's law (2.2).

Boundary value problems (2.3), (2.4); (2.3), (2.5) or, equivalently, (2.7), for a known function $\sigma(\mathbf{x})$ in Ω and its corresponding data $I(\mathbf{x})$ or $V(\mathbf{x})$, given for all $\mathbf{x} \in \partial\Omega$, are referred to as *forward* mathematical models for EIT.

2.2. The inverse problem

In EIT, the conductivity function $\sigma(\mathbf{x})$ is unknown and it is to be determined from simultaneous measurements of boundary voltages $V(\mathbf{x})$ and corresponding current densities $I(\mathbf{x})$. In this section, we define the DtN and NtD maps which relate $V(\mathbf{x})$ to $I(\mathbf{x})$. These maps depend nonlinearly on the unknown $\sigma(\mathbf{x})$ and they are the data in inversion. We review some properties of these maps and we formulate the inverse problem.

The DtN map $\Lambda_\sigma : H^{\frac{1}{2}}(\partial\Omega) \to H^{-\frac{1}{2}}(\partial\Omega)$ is defined as

$$\Lambda_\sigma V(\mathbf{x}) = \sigma(\mathbf{x})\frac{\partial\phi(\mathbf{x})}{\partial n} \qquad \text{for } \mathbf{x} \in \partial\Omega, \tag{2.8}$$

where $V(\mathbf{x})$ is arbitrary in $H^{\frac{1}{2}}(\partial\Omega)$ and $\phi(\mathbf{x})$ solves forward problem (2.3), (2.4). This map is self-adjoint and positive semidefinite with null space $\mathcal{N}\{\Lambda_\sigma\} = \{V(\mathbf{x}) = \text{constant}\}$ (see for example [19, 26, 98] and references therein). Moreover, it has the Dirichlet variational formulation [28]

$$\langle V, \Lambda_\sigma V\rangle = \min_{u|_{\partial\Omega}=V} \int_\Omega \sigma(\mathbf{x})|\nabla u(\mathbf{x})|^2\,\mathrm{d}\mathbf{x}, \qquad \text{for arbitrary } V(\mathbf{x}) \in H^{\frac{1}{2}}(\partial\Omega), \tag{2.9}$$

where $\langle\cdot,\cdot\rangle$ denotes the $L_2(\partial\Omega)$ inner product

$$\langle f, g\rangle = \int_{\partial\Omega} f(\mathbf{x})g(\mathbf{x})\,\mathrm{d}s(\mathbf{x}).$$

The mathematical formulation of EIT, as first posed by Calderón [23], is 'find a bounded, strictly positive conductivity function $\sigma(\mathbf{x})$, given the DtN map Λ_σ'. That this problem can be solved uniquely for a large class of functions σ is established in [35, 36, 71, 79, 97].

The generalized inverse of Λ_σ, the NtD map $(\Lambda_\sigma)^{-1} : \mathcal{J} \to H^{\frac{1}{2}}(\partial\Omega)$, is defined on the restricted space of currents

$$\mathcal{J} = \left\{ I(\mathbf{x}) \in H^{-\frac{1}{2}}(\partial\Omega) \text{ such that } \int_{\partial\Omega} I(\mathbf{x})\,\mathrm{d}s(\mathbf{x}) = 0 \right\} \tag{2.10}$$

and, for any $I(\mathbf{x}) \in \mathcal{J}$, $(\Lambda_\sigma)^{-1}I(\mathbf{x}) = \phi(\mathbf{x})$ at $\partial\Omega$, where $\phi(\mathbf{x})$ is the solution of Neumann boundary value problem (2.3), (2.5), (2.6). The NtD map $(\Lambda_\sigma)^{-1}$ is self-adjoint and positive definite [19, 26, 98], with Thomson variational formulation

$$\langle I, (\Lambda_\sigma)^{-1}I\rangle = \min_{\substack{\nabla\cdot\mathbf{j}=0 \\ -\mathbf{j}\cdot\mathbf{n}|_{\partial\Omega}=I}} \int_\Omega \frac{1}{\sigma(\mathbf{x})}|\mathbf{j}(\mathbf{x})|^2\,\mathrm{d}\mathbf{x}, \qquad \text{for arbitrary } I(\mathbf{x}) \in \mathcal{J} \tag{2.11}$$

(see for example [28]). Then, $(\Lambda_\sigma)^{-1}$ is the generalized inverse of Λ_σ, as can be seen from duality relations [17, 19, 38]

$$\langle V, \Lambda_\sigma V\rangle = \sup_{I\in\mathcal{J}}\{2\langle I, V\rangle - \langle I, (\Lambda_\sigma)^{-1}I\rangle\}, \qquad \text{for any } V(\mathbf{x}) \in H^{\frac{1}{2}}(\partial\Omega), \tag{2.12}$$

$$\langle I, (\Lambda_\sigma)^{-1}I\rangle = \sup_{V\in H^{\frac{1}{2}}(\partial\Omega)}\{2\langle I, V\rangle - \langle V, \Lambda_\sigma V\rangle\}, \qquad \text{for any } I(\mathbf{x}) \in \mathcal{J}. \tag{2.13}$$

In practice, we do not have full knowledge of maps $(\Lambda_\sigma)^{-1}$ or Λ_σ. Instead, we have a set of N *experiments*, where we define an excitation pattern $I_e(\mathbf{x}) \in \mathcal{J}$ and we measure the resulting voltage $V_e(\mathbf{x}_p)$, at discrete locations $\mathbf{x}_p \in \partial\Omega$ of the electrodes, along the boundary. Thus, the more realistic definition of EIT is 'find σ from partial and usually noisy knowledge of the NtD map'. A significant difficulty of the EIT problem is its severe ill-posedness which causes small perturbations of the boundary data to be *exponentially* amplified in the image of σ inside Ω [1, 6, 7, 19, 32, 34, 61, 76, 93, 99]. Consequently, all reconstruction methods must be stabilized by some regularization approach, which ensures convergence by restricting σ to a compact subset of $L^\infty(\Omega)$ (see for example [25, 39, 40, 51, 78, 100] or the statistical, Bayesian approaches in [66, 67, 83, 94, 103, 104]).

2.3. Variational feasibility constraints

Variational constraints on the conductivity function σ have been introduced by Berryman and Kohn [13], as follows:

Definition 1. *We say that function σ is Dirichlet feasible for boundary voltage $V_e \in H^{\frac{1}{2}}(\partial\Omega)$, if*

$$\langle V_e, \Lambda_\sigma V_e\rangle = \min_{u|_{\partial\Omega}=V_e} \int_\Omega \sigma(\mathbf{x})|\nabla u(\mathbf{x})|^2 \,\mathrm{d}\mathbf{x} \geqslant \langle V_e, \Lambda_{\sigma^\star} V_e\rangle, \tag{2.14}$$

where $\sigma^\star$ is the true conductivity and $\langle V_e, \Lambda_{\sigma^\star} V_e\rangle = \int_{\partial\Omega} V_e I_e \,\mathrm{d}s(\mathbf{x}) = P_e$ is the measured power dissipated into heat. Moreover, we say that σ is Dirichlet feasible, if (2.14) holds for all $V_e \in H^{\frac{1}{2}}(\partial\Omega)$, $e = 1, \ldots, N$.

The rationale behind this definition is given by variational principle (2.9), as follows: take any $\phi \in H^1(\Omega)$, such that $\phi|_{\partial\Omega} = V_e$, and obtain by (2.9)

$$\langle V_e, \Lambda_{\sigma^\star} V_e\rangle \leqslant \int_\Omega \sigma^\star(\mathbf{x})|\nabla\phi(\mathbf{x})|^2 \,\mathrm{d}\mathbf{x}. \tag{2.15}$$

Now, let $\phi = \phi_e$, the solution of Dirichlet problem (2.3), (2.4) for conductivity σ, and suppose that σ does not satisfy (2.14). Then,

$$\langle V_e, \Lambda_{\sigma^\star} V_e\rangle > \langle V_e, \Lambda_\sigma V_e\rangle = \min_{u|_{\partial\Omega}=V_e} \int_\Omega \sigma(\mathbf{x})|\nabla u(\mathbf{x})|^2 \,\mathrm{d}\mathbf{x} = \int_\Omega \sigma(\mathbf{x})|\nabla\phi_e(\mathbf{x})|^2 \,\mathrm{d}\mathbf{x}$$

and σ is deemed infeasible.

Similar to definition 1, we define the Thomson feasibility constraints as follows.

Definition 2. *A function σ is Thomson feasible for boundary electric current $I_e \in \mathcal{J}$, if*

$$\langle I_e, (\Lambda_\sigma)^{-1} I_e\rangle = \min_{\substack{\nabla\cdot\mathbf{j}=0 \\ -\mathbf{j}\cdot\mathbf{n}|_{\partial\Omega}=I_e}} \int_\Omega \sigma^{-1}(\mathbf{x})|\mathbf{j}(\mathbf{x})|^2 \,\mathrm{d}\mathbf{x} \geqslant \langle I_e, (\Lambda_{\sigma^\star})^{-1} I_e\rangle, \tag{2.16}$$

where $\langle I_e, (\Lambda_{\sigma^\star})^{-1} I_e\rangle = \int_{\partial\Omega} V_e I_e \,\mathrm{d}s(\mathbf{x}) = P_e$, the measured power dissipated into heat. Moreover, σ is Thomson feasible, if (2.16) holds for all $I_e \in \mathcal{J}$, $e = 1, \ldots, N$.

Finally, we say that σ is feasible if it is both Dirichlet and Thomson feasible.

3. Motivation for the variational formulation

Let us define the set of admissible conductivity functions

$$\mathcal{S} = \{\sigma(\mathbf{x}) \in L^\infty(\bar{\Omega}), \sigma(\mathbf{x}) \geqslant m\} \tag{3.1}$$

where m is some positive constant. Suppose that $\sigma^\star \in \mathcal{S}$ is the conductivity function to be imaged, such that, for a prescribed excitation current $I \in \mathcal{J}$, the boundary voltage is $V = (\Lambda_{\sigma^\star})^{-1} I$. Ideally, we would like to image the conductivity by minimizing the operator norm

$$\min_{\sigma\in\mathcal{S}} \|(\Lambda_\sigma)^{-1} - (\Lambda_{\sigma^\star})^{-1}\|_{H^{-\frac{1}{2}}(\partial\Omega), H^{\frac{1}{2}}(\partial\Omega)}, \tag{3.2}$$

but, since only limited data are available, we can consider at best

$$\min_{\sigma\in\mathcal{S}} \sum_{e=1}^{N} \|[(\Lambda_\sigma)^{-1} - (\Lambda_{\sigma^\star})^{-1}]I_e\|^2_{H^{\frac{1}{2}}(\partial\Omega)}, \qquad \text{for } I_e \in \mathcal{J}, \quad 1 \leqslant e \leqslant N, \tag{3.3}$$

for some positive integer N. Then, one could attempt to solve nonlinear problem (3.3) with an iterative optimization algorithm, such as Newton's method [30]. However, due to the high cost of computing fractional order Sobolev space norms and the possible lack of differentiability of the functional in (3.3) [27, 32, 33], no practical reconstruction algorithm uses formulation (3.3). Instead, one uses output least squares methods,

$$\min_{\sigma\in\mathcal{S}} \sum_{e=1}^{N} \|[(\Lambda_\sigma)^{-1} - (\Lambda_{\sigma^\star})^{-1}]I_e\|^2_{L^2(\partial\Omega)}, \tag{3.4}$$

where the objective function is an approximation of the Hilbert Schmidt norm of $(\Lambda_\sigma)^{-1} - (\Lambda_{\sigma^\star})^{-1}$ over $L^2(\partial\Omega)$ [32] (the currents I_e are scaled to unit norm). Obviously, formulation (3.4) can give at most a lower bound on (3.3) and, although numerically convenient, it could decrease the resolution of the image [27].

We propose to use the variational constraints, defined in definitions 1 and 2, to achieve the minimization (3.3) in a computationally efficient manner. A possible approach is suggested by the following lemma.

Lemma 1. *Let I and V be generic boundary data for imaging $\sigma^\star$ and let $\{\sigma_k(\mathbf{x})\}_{k\geqslant 1}$ be a sequence of functions in $\mathcal{S}$ such that*

$$\lim_{k\to\infty} \langle I, (\Lambda_{\sigma_k})^{-1} I\rangle = P \qquad \text{and} \qquad \lim_{k\to\infty} \langle V, \Lambda_{\sigma_k} V\rangle = P, \tag{3.5}$$

where $P = \langle I, V\rangle$. Then,

$$\lim_{k\to\infty} \|(\Lambda_{\sigma_k})^{-1} I - V\|_{H^{\frac{1}{2}}(\partial\Omega)} = 0. \tag{3.6}$$

Proof. Let us denote by ϕ_k the potential which solves forward problem (2.3), (2.4), for conductivity σ_k and Dirichlet data V. Also, let $\mathbf{j}_k$ be the electric current density which solves problem (2.7) for conductivity σ_k and Neumann data I. Equivalently, we have $\mathbf{j}_k = -\sigma_k\nabla\psi_k$, where ψ_k solves Neumann boundary value problem (2.3), (2.5), (2.6). Then, integration by parts and assumption (3.5) give

$$\langle I, (\Lambda_{\sigma_k})^{-1} I\rangle + \langle V, \Lambda_{\sigma_k} V\rangle - 2P = \int_\Omega \sigma_k(\mathbf{x})|\nabla\phi_k(\mathbf{x}) - \nabla\psi_k(\mathbf{x})|^2\,\mathrm{d}\mathbf{x} \to 0, \qquad \text{as } k\to\infty. \tag{3.7}$$

Moreover, by the coercivity of bilinear form $a(u, w) = \int_\Omega \sigma_k\nabla u\cdot\nabla w\,\mathrm{d}\mathbf{x}$, for $u, w\in H^1(\Omega)$ satisfying $\int_{\partial\Omega} u\,\mathrm{d}s = \int_{\partial\Omega} w\,\mathrm{d}s = 0$ [43], $\lim_{k\to\infty}\|\phi_k - \psi_k\|_{H^1(\Omega)} = 0$ and, by the trace theorem [43], $\lim_{k\to\infty}\|V - (\Lambda_{\sigma_k})^{-1} I\|_{H^{\frac{1}{2}}(\partial\Omega)} = 0$. □

Thus, we achieve the minimization (3.3), by seeking an inversion methodology which generates sequences $\{\sigma_k\}_{k\geqslant 1}$ of functions in $\mathcal{S}$ which satisfy the feasibility constraints of definitions 1 and 2 as equalities (or near equalities in the noisy case) in the limit $k\to\infty$. Such inversion methods are described in section 5.1 and they are based on the analysis of the variational constraints, which we give in section 4. Note in particular that $\mathbf{j}_k$ and ϕ_k are related by Ohm's law inside Ω (except possibly for subsets of measure zero), since, by (3.7), $\|\sigma_k\nabla\phi_k + \mathbf{j}_k\|_{L^2(\Omega)}\to 0$, as $k\to\infty$.

4. Analysis of variational constraints

4.1. Theory

As motivated by section 3, we wish to obtain, in a computationally efficient manner, a sequence $\{\sigma_k(\mathbf{x})\}_{k\geqslant 1}$ of conductivity functions satisfying (3.5). We begin by taking a closer look at output

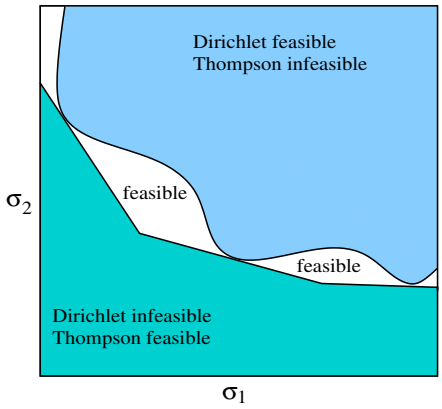

Figure 1. Take a planar section through the space of conductivity functions, where σ is parametrized in terms of two values σ_1 and σ_2. The Thomson infeasibility region is contained in the Dirichlet feasible region, as stated by lemma 2.

least squares methods, which generate sequences $\{\tilde{\sigma}_k(\mathbf{x})\}_{k\geqslant 1}$ of conductivities such that

$$\lim_{k\to\infty} \|(\Lambda_{\tilde{\sigma}_k})^{-1} I - V\|_{L^2(\partial\Omega)} = 0. \tag{4.1}$$

Since

$$\langle I, (\Lambda_{\tilde{\sigma}_k})^{-1} I\rangle - P = \int_{\partial\Omega} I[(\Lambda_{\tilde{\sigma}_k})^{-1} I - V]\,\mathrm{d}s,$$

output least squares can give convergence of the Thomson constraint,

$$\lim_{k\to\infty} \langle I, (\Lambda_{\tilde{\sigma}_k})^{-1} I\rangle = P,$$

provided that the excitation current I is taken in $L^2(\partial\Omega)$. Now, for the Dirichlet constraint, we have

$$\begin{aligned}
\langle V, \Lambda_{\tilde{\sigma}_k} V\rangle - P &= \langle V, \Lambda_{\tilde{\sigma}_k} V\rangle - \int_{\partial\Omega} V(\mathbf{x}) I(\mathbf{x})\,\mathrm{d}s(\mathbf{x}) \\
&= \langle V, \Lambda_{\tilde{\sigma}_k} V\rangle - \int_{\partial\Omega} \tilde{\phi}_k(\mathbf{x})\tilde{\sigma}_k(\mathbf{x})\frac{\partial\tilde{\psi}_k}{\partial n}(\mathbf{x})\,\mathrm{d}s(\mathbf{x}) \\
&= \langle V, \Lambda_{\tilde{\sigma}_k} V\rangle - \int_{\Omega} \nabla\cdot[\tilde{\sigma}_k(\mathbf{x})\tilde{\phi}_k(\mathbf{x})\nabla\tilde{\psi}_k(\mathbf{x})]\,\mathrm{d}\mathbf{x} \\
&= \langle V, \Lambda_{\tilde{\sigma}_k} V\rangle - \int_{\Omega} \nabla\cdot[\tilde{\sigma}_k(\mathbf{x})\tilde{\psi}_k(\mathbf{x})\nabla\tilde{\phi}_k(\mathbf{x})]\,\mathrm{d}\mathbf{x} \\
&= \int_{\partial\Omega} [V(\mathbf{x}) - (\Lambda_{\tilde{\sigma}_k})^{-1} I]\Lambda_{\tilde{\sigma}_k} V(\mathbf{x})\,\mathrm{d}s(\mathbf{x}),
\end{aligned}$$

where $\tilde{\phi}_k$ and $\tilde{\psi}_k$ are the Dirichlet and Neumann potentials solving problems (2.3), (2.4) and (2.3), (2.5), respectively, for conductivity $\tilde{\sigma}_k$ and data V and I. However, since $\Lambda_{\tilde{\sigma}_k} V \in H^{-\frac{1}{2}}(\partial\Omega)$, convergence of the Dirichlet constraint does not follow from (4.1).

To develop algorithms which give (3.5), we examine the relationship between the two feasibility constraints. We begin by showing that, given data I and V, which are in σ-correspondence, the Thomson infeasible set is included in the Dirichlet feasible set (see figure 1). Then, we could achieve convergence (3.5) of both constraints, to P, by confining all iterates σ_k to the Dirichlet infeasible region and by letting the Thomson constraint

converge to P. The latter can be achieved, for example, with output least squares, provided that we take I sufficiently smooth (in $L^2(\partial\Omega)$) (see sections 3 and 5.1).

Lemma 2. *Let $\sigma \in \mathcal{S}$ be a conductivity function satisfying $\langle I, (\Lambda_\sigma)^{-1} I\rangle \leqslant P$, for some $I \in \mathcal{J}$ and $P = \langle I, V\rangle$. Then, $\langle V, \Lambda_\sigma V\rangle \geqslant P$.*

Proof. The proof follows from duality relation (2.12). We have

$$\langle V, \Lambda_\sigma V\rangle \geqslant 2\langle I, V\rangle - \langle I, (\Lambda_\sigma)^{-1} I\rangle \geqslant 2\langle I, V\rangle - P = P.$$

Similarly, we obtain from duality relation (2.13) that the Dirichlet infeasible set in $\mathcal{S}$ is included in the Thomson feasible set, for data I and V. □

Lemma 3. *Let $\sigma \in \mathcal{S}$ be a conductivity function satisfying $\langle V, \Lambda_\sigma V\rangle \leqslant P$, for some $V \in H^{\frac{1}{2}}(\partial\Omega)$ and $P = \langle I, V\rangle$. Then, $\langle I, (\Lambda_\sigma)^{-1} I\rangle \geqslant P$.*

Note that, in general, given just one set of data I and its σ-corresponding voltage V, the interiors of the Dirichlet and Thomson feasible sets are not disjoint. To guarantee that the two sets intersect just at the boundary, we need all measurements, as stated below.

Lemma 4. *Let $\mathcal{D}$ and $\mathcal{T}$ be the interiors of the Dirichlet and Thomson feasibility sets, respectively,*

$$\mathcal{D} = \{\sigma \in \mathcal{S} \text{ such that } \langle V, \Lambda_\sigma V\rangle > \langle V, \Lambda_{\sigma^\star} V\rangle, \text{ for all } V \in H^{-\frac{1}{2}}(\partial\Omega)\}, \quad (4.2)$$

$$\mathcal{T} = \{\sigma \in \mathcal{S} \text{ such that } \langle I, (\Lambda_\sigma)^{-1} I\rangle > \langle I, (\Lambda_{\sigma^\star})^{-1} I\rangle, \text{ for all } I \in \mathcal{J}\}. \quad (4.3)$$

Then, $\mathcal{D} \cap \mathcal{T} = \emptyset$.

Proof. Suppose that $\sigma \in \mathcal{T}$, such that

$$2\langle I, V\rangle - \langle I, (\Lambda_\sigma)^{-1} I\rangle < 2\langle I, V\rangle - \langle I, (\Lambda_{\sigma^\star})^{-1} I\rangle,$$

for all $I \in \mathcal{J}$ and arbitrary $V \in H^{-\frac{1}{2}}(\partial\Omega)$. Taking the sup over I and using duality relation (2.12), we have

$$\langle V, \Lambda_\sigma V\rangle = \sup_{I\in\mathcal{J}}\{2\langle I, V\rangle - \langle I, (\Lambda_\sigma)^{-1} I\rangle\} \leqslant \sup_{I\in\mathcal{J}}\{2\langle I, V\rangle - \langle I, (\Lambda_{\sigma^\star})^{-1} I\rangle\} = \langle V, \Lambda_{\sigma^\star} V\rangle$$

and so $\sigma \notin \mathcal{D}$. In fact, if all measurements are available, by the uniqueness of solution of the inverse problem[4], the intersection of the feasibility sets consists of a single point $\sigma^\star$, the true solution. □

When using a reconstruction algorithm which confines all iterates σ_k inside (or outside) a feasibility set, one needs, for example, to find an appropriate initial guess. This can be easily done due to the monotonicity results.

Lemma 5. *Let σ, $\tilde{\sigma}$ be two functions in $\mathcal{S}$ and suppose that $\sigma(\mathbf{x}) \leqslant \tilde{\sigma}(\mathbf{x})$, for all $\mathbf{x}$ in Ω, with the possible exception of subsets of measure zero. Then,*

$$\langle V, \Lambda_\sigma V\rangle \leqslant \langle V, \Lambda_{\tilde{\sigma}} V\rangle \qquad \text{and} \qquad \langle I, (\Lambda_\sigma)^{-1} I\rangle \geqslant \langle I, (\Lambda_{\tilde{\sigma}})^{-1} I\rangle,$$

for any $V \in H^{\frac{1}{2}}(\partial\Omega)$ and $I \in \mathcal{J}$.

[4] Uniqueness has been proven for a large class of conductivities in [20, 35, 36, 71, 79, 84, 97]. All these results require some smoothness assumptions on σ but the result may hold for the entire set $\mathcal{S}$.

Proof. The proof is given by Berryman in [16]. We repeat it here, for completeness. From variational principle (2.9), we have

$$\langle V, \Lambda_\sigma V\rangle = \min_{u|_{\partial\Omega}=V} \int_\Omega \sigma(\mathbf{x})|\nabla u(\mathbf{x})|^2\,\mathrm{d}\mathbf{x} \leqslant \int_\Omega \sigma(\mathbf{x})|\nabla\tilde{\phi}(\mathbf{x})|^2\,\mathrm{d}\mathbf{x} \leqslant \int_\Omega \tilde{\sigma}(\mathbf{x})|\nabla\tilde{\phi}(\mathbf{x})|^2\,\mathrm{d}\mathbf{x}$$
$$= \min_{u|_{\partial\Omega}=V} \int_\Omega \tilde{\sigma}(\mathbf{x})|\nabla u(\mathbf{x})|^2\,\mathrm{d}\mathbf{x} = \langle V, \Lambda_{\tilde{\sigma}} V\rangle.$$

Similarly, from (2.11), we have

$$\langle I, (\Lambda_{\tilde{\sigma}})^{-1} I\rangle = \min_{\substack{\nabla\cdot\mathbf{i}=0\\ \mathbf{i}\cdot\mathbf{n}|_{\partial\Omega}=I}} \int_\Omega \frac{1}{\tilde{\sigma}(\mathbf{x})}|\mathbf{i}(\mathbf{x})|^2\,\mathrm{d}\mathbf{x}$$
$$= \int_\Omega \frac{1}{\tilde{\sigma}(\mathbf{x})}|\tilde{\mathbf{j}}(\mathbf{x})|^2\,\mathrm{d}\mathbf{x} \leqslant \int_\Omega \frac{1}{\tilde{\sigma}(\mathbf{x})}|\mathbf{j}(\mathbf{x})|^2\,\mathrm{d}\mathbf{x} \leqslant \int_\Omega \frac{1}{\sigma(\mathbf{x})}|\mathbf{j}(\mathbf{x})|^2\,\mathrm{d}\mathbf{x}$$
$$= \min_{\substack{\nabla\cdot\mathbf{i}=0\\ -\mathbf{i}\cdot\mathbf{n}|_{\partial\Omega}=I}} \int_\Omega \frac{1}{\sigma(\mathbf{x})}|\mathbf{i}(\mathbf{x})|^2\,\mathrm{d}\mathbf{x} = \langle I, (\Lambda_\sigma)^{-1} I\rangle.$$

□

We end this section with the well known convexity result (see for example [16, 64]).

Lemma 6. *Let $\sigma, \tilde{\sigma}$ be two functions belonging to the Dirichlet feasible set for data I and V. Then, the linear combination $\lambda\sigma + (1-\lambda)\tilde{\sigma}$, for $0 \leqslant \lambda \leqslant 1$, is Dirichlet feasible, as well.*

Note however that the set of Thomson feasible conductivities is not convex.

4.2. Examples

We give a few examples of the feasibility regions analysed in section 4.1, for a two-dimensional conductivity $\sigma(x, y)$ in a unit square Ω. We take $\sigma = 1$ everywhere in the domain, except for two rectangular inclusions, where σ equals σ_1 or σ_2. By varying σ_1 and σ_2, we obtain, similar to figure 1, a planar section through the space of conductivity functions. We calculate the Dirichlet and Thomson feasibility regions, for various data pairs (I, V) and different locations of the inhomogeneities inside Ω.

Let us inject unit current near the lower left corner of Ω and take it out near its upper right corner. For such a fixed I, we study the effect of the location of the inclusions on the feasibility regions. In figure 2, we have two inclusions, of conductivity $\sigma_1 = 2$ and $\sigma_2 = 0.5$, near the centre of the domain. We show in the right-hand picture the feasibility region (the intersection of the Dirichlet and Thomson feasibility regions), for data I and corresponding data V. Note that the feasibility region collapses to a long arc in the part of the plane displayed in the figure. Any pair (σ_1, σ_2) along this arc gives an almost perfect fit of the data, and so the conductivity distribution in figure 2 cannot be determined by just this experiment I, V. However, as shown in figure 3, inclusions which are close to the boundary are easily distinguished, because the boundaries of the Dirichlet and Thomson feasibility regions intersect at one point, the exact conductivity.

Next, we fix the conductivity distribution to that shown in figure 4, where we have two inclusions of conductivity $\sigma_1 = 2$ and $\sigma_2 = 0.5$ in a background of unit conductivity, and we study the effect of the excitation current on the feasibility set. In the middle picture of figure 4 we take the optimal current which best distinguishes the inclusions in Ω [27, 61], whereas in the right-hand picture of figure 4 we inject and take out unit current near the upper left and lower right corners of Ω, respectively. As seen from figure 4, the latter is a bad excitation,

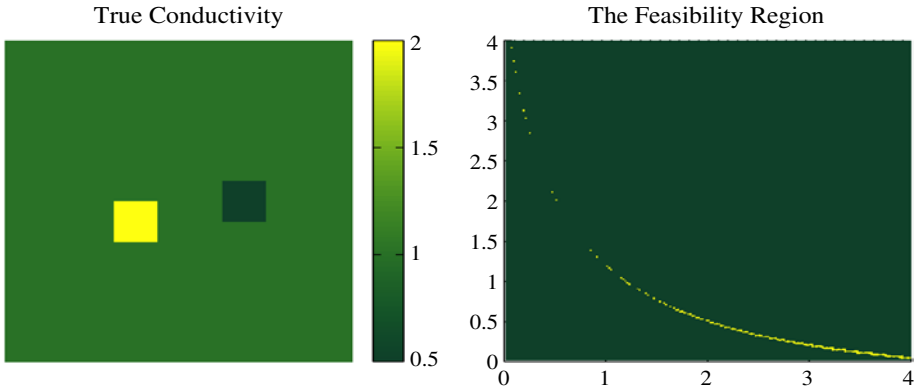

Figure 2. On the left, we plot σ as a function of x and y. On the right, we show in yellow the feasibility region in the plane parametrized by σ_1 and σ_2. The conductivity distribution on the left is not easily distinguishable by the experiment with data (I, V), because the boundaries of the two feasibility regions intersect along a long arc in the plane.

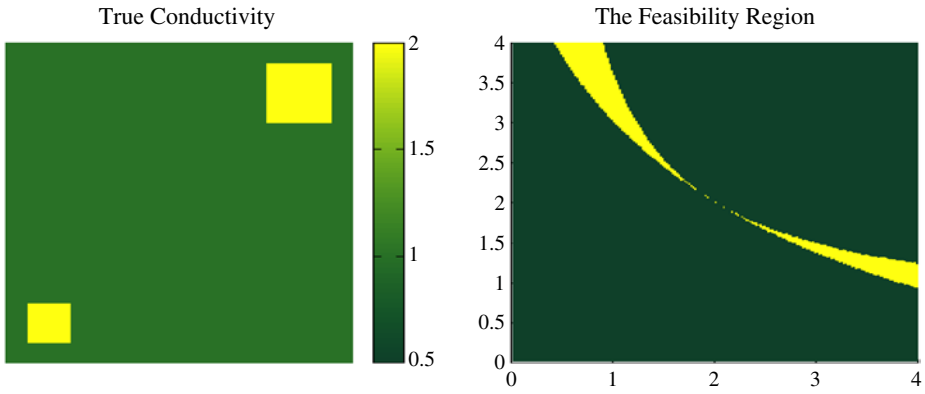

Figure 3. The conductivity distribution on the left is easily distinguishable by the experiment I, V, because the boundaries of the two feasibility regions intersect just at one point, where the true solution lies.

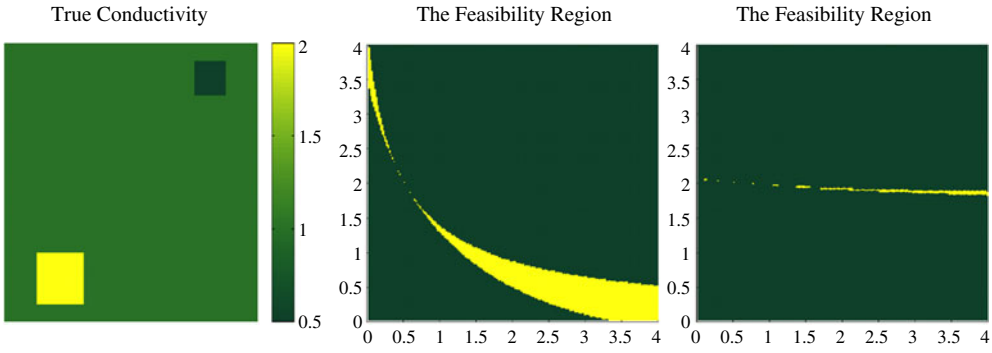

Figure 4. The conductivity distribution in the left-hand picture can be easily distinguished with the optimal current excitation, but it cannot be distinguished by a bad example of a current excitation.

which cannot distinguish the conductivity, since the feasibility region collapses to a long arc over a large region in the plane (σ_1, σ_2).

Clearly, for more general conductivity distributions, it is typically not possible to find σ with just one experiment, and so more data are needed and one should look at the intersection of the feasibility regions for all available current excitations. This could be useful, in particular, in special cases where the conductivity is known *a priori* to be piecewise constant over M given subdomains (i.e. σ is parametrized in terms of $\sigma_1, \sigma_2, \ldots, \sigma_M$)[Note 5], because we could use the feasibility constraints to determine the error in the recovered σ_j, for $j = 1, \ldots, M$.

5. Variationally constrained reconstruction algorithms

In this section, we introduce several variational algorithmic approaches for the numerical solution of the EIT problem. Then, we describe in detail our implementation of two variational algorithms and the unconstrained output least squares algorithm.

5.1. Several algorithmic approaches

We assume that N experiments have been conducted with boundary excitation currents $I_e \in \mathcal{J}$, that the corresponding voltages V_e at $\partial\Omega$ have been measured[6] and that the power dissipated into heat, $P_e = \int_{\partial\Omega} I_e V_e \, \mathrm{d}s$, has been estimated, for $e = 1, 2, \ldots, N$.

5.1.1. Constrained least squares approach. As is shown in section 3, in the output least squares formulation, for $I_e \in \mathcal{J} \bigcap L^2(\partial\Omega)$, the convergence of objective function (3.4) to zero implies the convergence of the Thomson constraint, to P_e, but not necessarily that of the Dirichlet constraint. However, in light of the results in section 4.1, we can achieve the desired convergence (3.5) of both Dirichlet and Thomson constraints on σ, by the *constrained least squares* approach:

$$\min_{\sigma\in\mathcal{S}} \sum_{e=1}^{N} \|(\Lambda_\sigma)^{-1} I_e - V_e\|^2_{L^2(\partial\Omega)} \qquad \text{s.t. } \langle V_e, \Lambda_\sigma V_e\rangle \leqslant P_e, \quad e = 1, \ldots, N, \tag{5.1}$$

where $I_e \in \mathcal{J} \bigcap L^2(\partial\Omega)$ and $V_e = (\Lambda_{\sigma^\star})^{-1} I_e \in H^{\frac{1}{2}}(\partial\Omega)$. By requiring σ to be in the Dirichlet infeasibility region, we ensure that, at the minimizer, both Dirichlet and Thomson constraints are satisfied as equalities (or near equalities in the presence of noise). Equivalently, a minimizer of (5.1) lies at the intersection between the Dirichlet and Thomson feasibility boundaries. Furthermore, by minimizing over the set $\mathcal{S}$ defined in (3.1), we require that σ be strictly positive.

5.1.2. Equation error approach. If follows from the proof of lemma 1 that

$$\langle V_e, \Lambda_\sigma V_e\rangle + \langle I_e, (\Lambda_\sigma)^{-1} I_e\rangle - 2P_e = \int_\Omega \sigma(\mathbf{x}) |\nabla[\psi_e(\mathbf{x}) - \phi_e(\mathbf{x})]|^2 \, \mathrm{d}\mathbf{x} \geqslant 0, \tag{5.2}$$

where ϕ_e is the solution of Dirichlet problem (2.3) and (2.4), with data $V_e = (\Lambda_{\sigma^\star})^{-1} I_e \in H^{\frac{1}{2}}(\partial\Omega)$, and ψ_e is the solution of Neumann problem (2.3) and (2.5), with data $I_e \in \mathcal{J}$. Then,

[5] Such problems may arise in medical imaging, where the borders of the subdomains of constant conductivity could be determined from CAT scans [65].

[6] Note that, in all our reconstructions, I_e and V_e are given at *discrete* locations along $\partial\Omega$. Hence, for the numerical solution of the forward problems and for the calculation of P_e, we use these discrete data points and construct a quadrature to evaluate the pertinent integrals.

a global minimizer of

$$\min_{\sigma\in\mathcal{S}} \sum_{e=1}^{N} (\langle V_e, \Lambda_\sigma V_e\rangle + \langle I_e, (\Lambda_\sigma)^{-1} I_e\rangle - 2P_e) \tag{5.3}$$

is a solution of the EIT problem, at which Ohm's law $\mathbf{j}_e = -\sigma\nabla\psi_e = -\sigma\nabla\phi_e$ is satisfied (in the $L^2(\Omega)$ sense), at least for noiseless data. In this formulation, we again require that σ be strictly positive by minimizing over the set $\mathcal{S}$. We note that this approach is equivalent to that of [70, 73, 105] and, as such, we refer to it as the equation-error variational formulation.

5.1.3. Other approaches. Since the Dirichlet infeasibility region for data pair (I, V) is a subset of the Thomson feasibility region for the same data pair (see section 4.1), the minimization of Thomson functional $\langle I_e, (\Lambda_\sigma)^{-1} I_e\rangle - P_e \geqslant 0$, over Dirichlet infeasible σ, ensures the desired convergence (3.5). Explicitly, we take

$$\min_{\sigma\in\mathcal{S}} \sum_{e=1}^{N} (\langle I_e, (\Lambda_\sigma)^{-1} I_e\rangle - P_e) \qquad \text{s.t. } \langle V_e, \Lambda_\sigma V_e\rangle \leqslant P_e, \quad e = 1, \ldots, N, \tag{5.4}$$

for $I_e \in \mathcal{J}$ and $V_e = (\Lambda_{\sigma^\star})^{-1} I_e \in H^{\frac{1}{2}}(\partial\Omega)$. Similarly, we can have a 'dual' formulation, where we constrain σ to the Thomson infeasibility region and we minimize the Dirichlet functional $\langle V_e, \Lambda_\sigma V_e\rangle - P_e \geqslant 0$:

$$\min_{\sigma\in\mathcal{S}} \sum_{e=1}^{N} (\langle V_e, \Lambda_\sigma V_e\rangle - P_e) \qquad \text{s.t. } \langle I_e, (\Lambda_\sigma)^{-1} I_e\rangle \leqslant P_e, \quad e = 1, \ldots, N. \tag{5.5}$$

In addition, there exist other possibilities. For example, one may directly seek to find a conductivity in the intersection of the Thomson and Dirichlet feasibility boundaries by minimizing the distance between the two infeasibility regions:

$$\min_{\sigma_{\mathrm{D}},\sigma_{\mathrm{T}}} \|\sigma_{\mathrm{D}} - \sigma_{\mathrm{T}}\|^2_{L^2(\Omega)} \qquad \text{s.t. } \langle V_e, \Lambda_{\sigma_{\mathrm{D}}} V_e\rangle \leqslant P_e, \quad \langle I_e, (\Lambda_{\sigma_{\mathrm{T}}})^{-1} I_e\rangle \leqslant P_e, \quad e = 1, \ldots, N. \tag{5.6}$$

Here, σ_{D} is in the Dirichlet infeasibility region and σ_{T} in the Thompson infeasibility region. The reconstruction can then be given by the pointwise average of σ_{D} and σ_{T}.

Although the formulations based on variational constraints are 'equivalent' in a mathematical sense (i.e. they perform essentially the same data fit), their practical performance may differ from case to case. Our numerical experiments suggest that approaches (5.1), (5.4) and (5.5) perform similarly in the tested cases, and that they are the most consistent ones of all the formulations that we have considered. The equation-error approach (5.3) performs equally well for noiseless data but it can behave differently for noisy measurements. Finally, approach (5.6) is the least successful one. Our preliminary studies suggest that the objective function in (5.6) has many local minima and, as such, the iterative optimization process stagnates after just a few steps, for most initial guesses. Due to this behaviour, we have not been able to obtain reasonable reconstructions with formulation (5.6), at least for realistic initial starting values of σ.

5.2. Implementation

We now describe our implementation of three formulations: (1) the constrained least squares approach, (2) the equation-error approach and (3) the unconstrained output least squares approach. We choose the constrained least squares approach to represent the newly proposed variationally constrained formulations, and we compare it with the other two approaches.

5.2.1. The optimization method. In an attempt to achieve better scaling, we have implemented normalized versions of the three formulations: namely, the normalized constrained least squares formulation,

$$\min_{\sigma\in\mathcal{S}} \sum_{e=1}^{N} \frac{\|(\Lambda_\sigma)^{-1} I_e - V_e\|^2_{L^2(\partial\Omega)}}{\|V_e\|^2_{L^2(\partial\Omega)}} \qquad \text{s.t. } \langle V_e, \Lambda_\sigma V_e\rangle \leqslant P_e, \quad e = 1, \ldots, N, \tag{5.7}$$

the normalized equation-error formulation,

$$\min_{\sigma\in\mathcal{S}} \sum_{e=1}^{N} \frac{\langle V_e, \Lambda_\sigma V_e\rangle + \langle I_e, (\Lambda_\sigma)^{-1} I_e\rangle - 2P_e}{2P_e}, \tag{5.8}$$

and the normalized unconstrained output least squares formulation,

$$\min_{\sigma\in\mathcal{S}} \sum_{e=1}^{N} \frac{\|(\Lambda_\sigma)^{-1} I_e - V_e\|^2_{L^2(\partial\Omega)}}{\|V_e\|^2_{L^2(\partial\Omega)}}. \tag{5.9}$$

Furthermore, in each of the above formulations, by minimizing over the set of all $\sigma \in \mathcal{S}$, we are requiring σ to be strictly positive. This condition could be enforced by explicitly adding the constraint $\sigma \geqslant m$, where m is some small positive constant, to each formulation. However, we implemented (5.8) and (5.9) without this constraint because no iterate σ was ever produced in our experiments that was not strictly positive. Moreover, we did not add this additional constraint to our implementation of formulation (5.7) since we found that, for our experiments, it was always the case that $\sigma > 0$ whenever a feasible initial guess was used.

To solve the optimization problems (5.7)–(5.9), we use routines from OPT++, a library of nonlinear optimization algorithms written in C++ [55]. Since the goal of our numerical study is to validate the variational formulations, we employ existing software to demonstrate that implementing the constrained least squares formulation is both reasonable and practical. Using existing software also eliminates any biases that may occur in customized optimization routines and allows us to make fair comparisons of the methods.

Solving an optimization problem with OPT++ requires the user to select an optimization method and to set several algorithm inherent parameters. For formulation (5.7), we opted to use the nonlinear interior point solver NIPS, the only method available in OPT++ that is capable of handling nonlinear constraints. To solve the unconstrained formulations (5.8) and (5.9), both NIPS[7] and the OPT++ quasi-Newton methods are appropriate choices. We tested both methods but saw no significant difference in the reconstructions obtained. Thus, for consistency of the comparisons, all the results we present here were obtained using NIPS.

To measure the progress of its optimization algorithm, OPT++ uses a merit function. Merit functions are particularly useful when solving constrained nonlinear optimization problems such as (5.7) because they strike a balance between reducing the objective function and satisfying the constraints. OPT++ offers the user three options for the merit function: the VanShannon, the ArgaezTapia, and the norm of the KKT conditions (NormFmu) [55]. We tested all three available choices and found NormFmu to be the most useful for our problems. Note that, for formulations (5.8) and (5.9), NormFmu corresponds to the norm of the gradient of the function, not to the function itself, which is often the choice for a merit function for an unconstrained problem. Because nonlinear optimization has been studied extensively, we refer the reader to the literature for further details on merit functions (see for example chapter 15 in [80] and references therein).

Finally, all the optimization algorithms in OPT++ require the user to define some stopping criteria. Using numerical experiments, we chose the maximum number of iterations to be 100,

[7] For unconstrained problems, NIPS corresponds to the BFGS method (see for example chapter 8 of [80] and references therein).

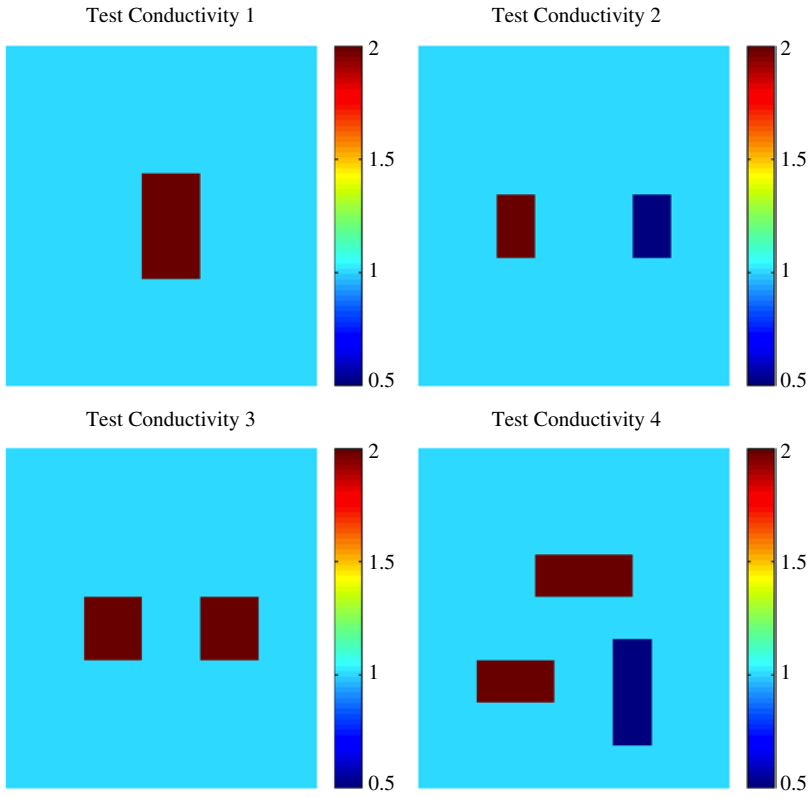

Figure 5. The four conductivity models used in the numerical study.

and the maximum number of function evaluations to be 1000. We also required the algorithm to stop whenever the norm of the gradient of the merit function became smaller than 10^{-8}. In OPT++, this stopping criterion is called the function tolerance and it is set as an input parameter. To prevent bias in our comparisons, we used the same stopping tolerances for all three algorithms.

5.2.2. Discretization and calculation of derivatives. In our implementation, we only consider the two-dimensional problem with the domain Ω being the unit square. This simple model allows a straightforward implementation and manageable computational times, while being adequate for the purpose of evaluating the strength and weakness of different formulations. For convenience, we assume that the conductivity is known at the boundary of the domain. In all simulations included in this paper, we discretize the conductivity in terms of its nodal values, as a piecewise linear function, on a 16×16 uniform mesh of Ω. Note that because of the ill-posedness of the inverse problem, discretizing σ on a finer grid would not be advantageous. On the boundary, σ is set to be the constant unity (1.0) at each of the 64 boundary nodes. The unknowns are the values of the conductivity at each of the 225 interior nodes.

We use the first N optimal current excitation vectors as described in [26, 46, 61]. These N currents are the eigenvectors corresponding to the N largest in magnitude eigenvalues of the real symmetric matrix given by the difference between the discrete NtD maps for true σ and for $\sigma^0 = 1$. The procedure for determining these eigenvectors and for selecting N is discussed in detail in appendix C of [48]. In our experiments, we set $N = 15$, 18, 19 and 23 for test conductivity models 1–4, respectively, illustrated in figure 5.

For each experiment, we solve the Dirichlet and Neumann problems for the current conductivity, at any iterate σ, on a 32×32 uniform triangularization of the domain Ω using the piecewise linear, finite elements method. The reason for using a finer mesh for the forward problems than for the inverse problem is that the extra accuracy in solving the forward problems is expected to lead to more accurate functional and gradient values, hence hopefully enhancing the quality and robustness of the inversion. Since our goal in this numerical study is merely to demonstrate the merit of the variational formulations, we only note that the forward problem can be easily solved on a finer grid but opt to use a 32×32 discretization of Ω.

The quadrature rules for the approximation of the constraints are defined such that the important identity (5.2) is preserved as much as possible in the discrete setting. Let us denote by $\bar{G} = G \cup \partial G$ the grid for the numerical solution of the forward problems, where G is the set of interior grid points and ∂G is the set of boundary points. The Neumann potential ψ is given by

$$\psi(\mathbf{x}) = \sum_{j \in \bar{G}} \psi_j b_j(\mathbf{x}), \tag{5.10}$$

where $b_j(\mathbf{x})$ are the usual piecewise linear basis functions for the uniform triangulation on $\bar{G}$ and ψ_j are the unknown values of ψ at the grid points $j \in \bar{G}$, calculated such that

$$\int_\Omega \sigma(\mathbf{x}) \nabla v(\mathbf{x}) \cdot \nabla \psi(\mathbf{x})\, \mathrm{d}\mathbf{x} = \int_{\partial\Omega} I(\mathbf{x}) v(\mathbf{x})\, \mathrm{d}s(\mathbf{x}), \text{ for all piecewise linear functions } v(\mathbf{x}). \tag{5.11}$$

Then, by setting $v(\mathbf{x}) = \psi(\mathbf{x})$ in (5.11), we obtain for the Thomson constraint

$$\langle I, (\Lambda_\sigma)^{-1} I \rangle \approx \sum_{j \in \partial G} \psi_j \int_{\partial\Omega} I(\mathbf{x}) b_j(\mathbf{x})\, \mathrm{d}s(\mathbf{x}) = \int_\Omega \sigma(\mathbf{x}) |\nabla \psi(\mathbf{x})|^2\, \mathrm{d}\mathbf{x}. \tag{5.12}$$

The Dirichlet potential ϕ is given by

$$\phi(\mathbf{x}) = \sum_{j \in \partial G} V_j b_j(\mathbf{x}) + \sum_{j \in G} \phi_j b_j(\mathbf{x}), \tag{5.13}$$

where V_j is the given voltage at $j \in \partial G$ and where ϕ_j, for $j \in G$, are calculated such that

$$\int_\Omega \sigma(\mathbf{x}) \nabla v(\mathbf{x}) \cdot \nabla \phi(\mathbf{x})\, \mathrm{d}\mathbf{x} = 0, \text{ for all piecewise linear functions } v(\mathbf{x}) \text{vanishing at } \partial G. \tag{5.14}$$

Taking $v(\mathbf{x}) = \phi(\mathbf{x})$ in (5.11), we have

$$P = \langle I, V \rangle \approx \sum_{j \in \partial G} V_j \int_{\partial\Omega} I(\mathbf{x}) b_j(\mathbf{x})\, \mathrm{d}s(\mathbf{x}) = \int_\Omega \sigma(\mathbf{x}) \nabla \psi(\mathbf{x}) \cdot \nabla \phi(\mathbf{x})\, \mathrm{d}\mathbf{x}. \tag{5.15}$$

Finally, from (5.14), taking $v(\mathbf{x}) = \phi(\mathbf{x}) - \sum_{j \in \partial G} V_j b_j(\mathbf{x})$, we have

$$\langle V, \Lambda_\sigma V \rangle \approx \sum_{j \in \partial G} V_j \int_\Omega \sigma(\mathbf{x}) \nabla b_j(\mathbf{x}) \cdot \nabla \phi(\mathbf{x})\, \mathrm{d}\mathbf{x} = \int_\Omega \sigma(\mathbf{x}) |\nabla \phi(\mathbf{x})|^2\, \mathrm{d}\mathbf{x}, \tag{5.16}$$

where the integration on the left-hand side is limited to the triangles with at least one node in ∂G.

We note that formulations and (5.7), (5.8) require the solutions of both Dirichlet and Neumann problems, while in the unconstrained output least squares (5.9) formulation, only the Neumann problem needs to be solved. Nevertheless, the stiffness matrices A_D and A_N that one inverts in the numerical solution of Dirichlet and Neumann problems (5.14) and (5.11), respectively, are closely related to each other. In fact, A_D is a subblock of A_N and this

can be used toward reducing the computational cost[8]. Therefore, although the constrained least squares formulation is computationally more expensive to solve than its unconstrained counterpart, it is still affordable. In section 6, we will give some preliminary results that show that this extra computation is also worthwhile because it yields better quality results.

An important computational task in our implementation is the evaluation of the first derivatives of the objective functionals. An efficient computation of the derivatives is given by the adjoint method (see for example [33]). Straightforward calculations [48] give that the first derivative of $\langle V, \Lambda_\sigma V\rangle$, with respect to σ, is given, pointwise for $\mathbf{x} \in \Omega$, by

$$(\mathcal{D}\langle V, \Lambda_\sigma V\rangle)(\mathbf{x}) = |\nabla\phi(\mathbf{x})|^2 \tag{5.17}$$

and it is thus based solely on the previously computed approximation of ϕ, the solution of the Dirichlet problem for conductivity σ. The derivative of $\langle I, (\Lambda_\sigma)^{-1} I\rangle$, with respect to σ, is given, pointwise for $\mathbf{x} \in \Omega$, by [48]

$$(\mathcal{D}\langle I, (\Lambda_\sigma)^{-1} I\rangle)(\mathbf{x}) = -|\nabla\psi(\mathbf{x})|^2, \tag{5.18}$$

where ψ is the Neumann potential. Finally, the derivative of the output least squares functional is

$$(\mathcal{D}\|(\Lambda_\sigma)^{-1} I - V\|^2_{L^2(\partial\Omega)})(\mathbf{x}) = -2\nabla\psi(\mathbf{x}) \cdot \nabla\tau(\mathbf{x}), \tag{5.19}$$

where τ is the (piecewise linear) adjoint potential satisfying

$$\int_\Omega \sigma(\mathbf{x})\nabla v(\mathbf{x}) \cdot \nabla\tau(\mathbf{x})\, \mathrm{d}\mathbf{x} = \int_{\partial\Omega} [(\Lambda_\sigma)^{-1} I(\mathbf{x}) - V(\mathbf{x})] v(\mathbf{x})\, \mathrm{d}s(\mathbf{x})$$

for all piecewise linear functions $v(\mathbf{x})$. The calculation of τ and ψ require the inversion of the same stiffness matrix A_N, so (5.19) is calculated with little extra computation.

The function, constraint and derivative calculations for all three algorithms were implemented as Fortran 90 subroutines. We use the software package SuperLU [8, 29] to efficiently solve the sparse linear systems resulting from the finite-element discretization. These subroutines are accessed by the OPT++ optimization routines via customized wrappers [55].

6. Numerical results

In this section, we present numerical results and we compare the performance of the three implemented algorithms (see section 5.2). We reiterate that the objective of our numerical comparison is to evaluate the reconstruction quality of these algorithms. Therefore, we will not include CPU in the presented results. Although our current implementations are adequately efficient for all three algorithms, there certainly exists ample room for further improvements. Moreover, the question of which optimization methods are most effective for the approaches we have presented remains a topic for further study. However, we will make reference to the 'wall clock time' (i.e. the elapsed time between when the process starts to run and when it is finished) as reported by OPT++. These times will show that although the variational methods are more expensive, they are still affordable. Note that all the numerical tests were run on an Alpha Ev6 Linux machine based on Redhat Linux 6.2, using a stock 2.2.18 Linux kernel.

To make a fair comparison, we use the same simulated data for all three methods, and we start each algorithm from the same initial guess, conductivity $\sigma^0 \equiv 1$ at all nodes. However, for the constrained least squares formulation, such an initial guess may not be feasible with respect to the constraints $\langle V_e, \Lambda_\sigma V_e\rangle \leqslant P_e$ for $e = 1, 2, \ldots, N$. In this case, invoking the

[8] For example, one can use a block factorization approach where, once A_D has been factorized, A_N can be factorized at a small extra cost (see [47], for example).

monotonicity of the Dirichlet constraint (lemma 5), we decrease the value of σ^0 at all the interior nodes of Ω until the constraints are strictly satisfied.

We test the three algorithms on four different conductivity models as illustrated in figure 5. All four models have a background conductivity equal to unity. The first model contains a single inclusion with conductivity value equal to 2; the second contains two inclusions with conductivity values equal to 2 and $1/2$, respectively; the third contains two inclusions, both with conductivity values equal to 2; and the fourth model contains three separate inclusions, two with conductivity values equal to 2 and one with a conductivity value equal to $1/2$.

6.1. Regularization

The variational constraints restrict the space of admissible conductivity functions and, as such, they may introduce some natural regularization to the problem. However, the ill-posedness is not eliminated by the variational constraints, as one can see easily from well known counter examples (see for example [6]). Initial testing of our algorithms showed that further regularization is needed for better performance[9]. We thus take a Tikhonov type regularization [101], where we add to each objective function the regularization term

$$\alpha \|\nabla \sigma\|^2_{L^2(\Omega)}, \tag{6.1}$$

for a small, positive parameter α. This ensures that $\sigma - \sigma^0 \in H^1_0(\Omega)$, where σ^0 is the initial guess. Then, by the compact embedding $H^1_0(\Omega) \subset\subset L^2(\Omega)$ [2], we have that any sequence of iterates $\{\sigma^k\}$ contains at least a subsequence $\{\sigma^{k_l}\}$ which converges strongly in $L^2(\Omega)$, to σ_α, a minimizer of the regularized objective function.

Clearly, there are many other possible regularization methods (see for example [9, 39, 41, 50, 51, 74, 77, 101] and the references therein). However, our investigation focuses on the performance of the variational formulations, rather than on the choice of regularization. Thus, we take a convenient regularization method, which is inexpensive and easy to implement.

The parameter α is chosen with the Morozov discrepancy principle [39, 77, 86], implemented numerically via the practical procedure suggested in [9]. We begin with a relatively large value for α and, as the algorithm progresses, we gradually decrease α until the value of the objective function is less than some specified tolerance ε. In our implementation, we chose to reduce α by one order of magnitude whenever the regularization term dominated the objective function. In the case of noiseless data, the tolerance ε reflects numerical error. When noise is present, the tolerance is chosen so as to avoid fitting the noise in the data. For both the output least squares and constrained least squares methods, the inequality to be satisfied is

$$\sum_{e=1}^{N} \frac{\|(\Lambda_\sigma)^{-1} I_e - V_e\|^2_{L^2(\partial\Omega)}}{\|V_e\|^2_{L^2(\partial\Omega)}} \leqslant \varepsilon. \tag{6.2}$$

Since the stopping criterion is the same for these two methods, we choose the same regularization parameter for both methods. For the equation-error method, α is reduced until

$$\sum_{e=1}^{N} \frac{(\langle V_e, \Lambda_\sigma V_e\rangle + \langle I_e, (\Lambda_\sigma)^{-1} I_e\rangle - 2P_e)}{2P_e} \leqslant \varepsilon. \tag{6.3}$$

[9] For example, if we examine the objective function near the computed solution, we observe the following manifestation of the ill-posedness of the EIT problem: without additional regularization, the objective function appears to be very flat so that two conductivity distributions may attain approximately the same objective function value, but differ significantly from one another. The addition of a regularization term makes the function appear more 'curved' and it thus reduces the severity of ill-conditioning.

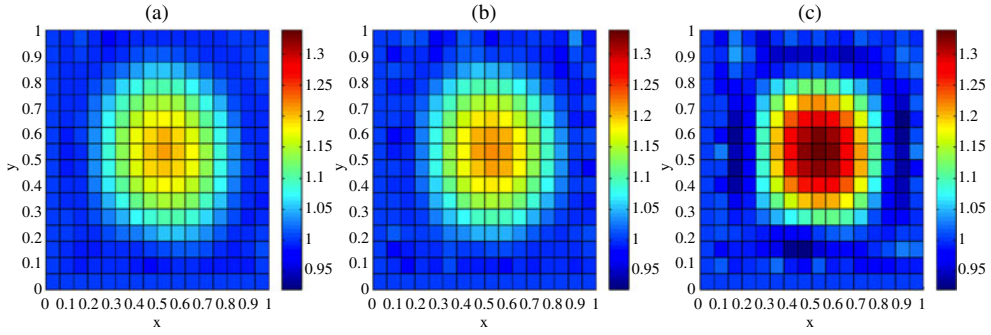

Figure 6. Reconstructions of test conductivity 1. Noise level: 1%. (a) Output least squares; (b) equation error; (c) constrained least squares.

Because the equation-error method has a very different objective functional, its regularization parameter α may differ from that of the output least squares and constrained least squares methods. For the purposes of our comparison study, we compute the ε in (6.3) by calculating the left-hand side of (6.3) with noisy data for a known conductivity. Although this way of choosing the tolerance works only in simulation studies, we use it to ensure that we do our best to choose the parameter ε for the equation-error method, in order to have a fair comparison. Note that, for all three methods, the values of ε were incorporated into OPT++ using the 'function tolerance' parameter which is one of the input parameters.

6.2. *Noisy data*

In practice, EIT data are contaminated with noise. Hence we test the three algorithms using noisy data at a 1% noise level and a 3% noise level. Past studies have considered data with noise levels as high as 20% (see for example [53, 106]). However, most algorithms tend to perform very poorly with such inaccurate data. Furthermore, with today's technology, it is expected that the noise level in EIT data be small[10].

We add uniformly distributed, multiplicative random noise to each of the vectors of boundary potentials, $\mathbf{V_e}$, for $e = 1, \ldots, N$. Thus, for each experiment e, the voltage data are now

$$V_e(i) = V_e(i) + \frac{\xi}{100}\varphi_i |V_e(i)| \tag{6.4}$$

where $V_e(i)$ is the ith component of vector $\mathbf{V_e}$, corresponding to the ith boundary point, ξ is the strength of the noise, and φ_i is a random number from a uniform distribution in [0,1] generated by the function `RANDOM_NUMBER` intrinsic to Fortran 90.

6.2.1. Numerical results with 1% noise. Figure 6 shows the reconstructions of test conductivity 1 obtained with data at a 1% noise level. All three methods produce a smooth image without spurious artifacts. However, the magnitude of the inclusion obtained by the constrained least squares is significantly higher than that of the other two methods. For this test, the wall clock time of the output least squares method was 56 s while the wall clock

[10] A discussion of measurement accuracy in real data gathering experiments can be found, for example, in [87]. Given the present modern equipment, the noise level expected is around 1%. Nevertheless, the number 1% is not always accurate and it may be site and application dependent. In particular, measurements for medical imaging applications [54] are usually more accurate than those in geophysics.

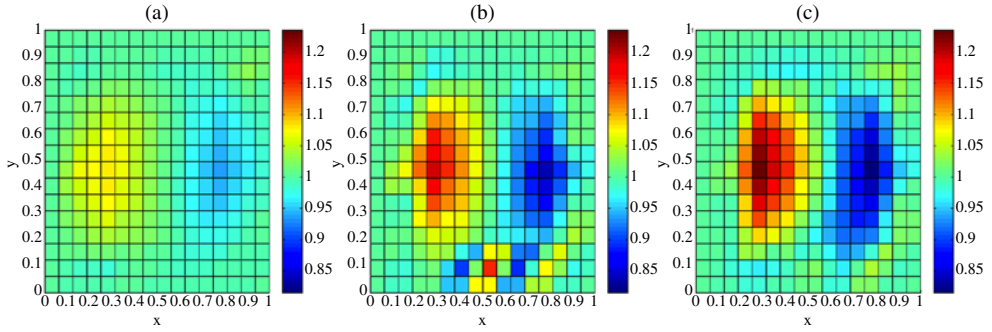

Figure 7. Reconstructions of test conductivity 2. Noise level: 1%. (a) Output least squares; (b) equation error; (c) constrained least squares.

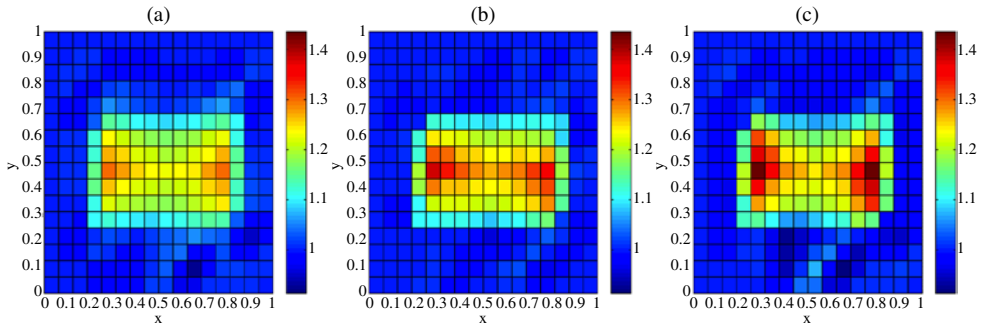

Figure 8. Reconstructions of test conductivity 3. Noise level: 1%. (a) Output least squares; (b) equation error; (c) constrained least squares.

time of the constrained least squares method was 142 s. Although it took the constrained least squares algorithm more than twice as long to find a solution, it should be noted that it found a better solution in a reasonable amount of time.

The recovered images of test conductivity 2 are displayed in figure 7. The magnitudes obtained by the variational methods are better than those of the output least squares algorithm. The equation-error method shows a few spurious artifacts while both least squares methods are quite smooth. Note that both least squares methods begin with the same regularization parameter, $\alpha = 10^{-4}$. This is subsequently reduced to $\alpha = 10^{-7}$.

The reconstructed images of test conductivity 3 are given in figure 8. All three methods are able to fit the boundary data so that

$$\sum_{e=1}^{N} \frac{\|(\Lambda_\sigma)^{-1} I_e - V_e\|^2_{L^2(\partial\Omega)}}{\|V_e\|^2_{L^2(\partial\Omega)}} \sim \mathcal{O}(10^{-5}).$$

However, the variational methods do a better job of distinguishing between the two inclusions. Again, the wall clock times of the variational methods were twice that of output least squares. However, solutions to the variational formulations were obtained in approximately four minutes each which is still quite affordable.

Figure 9 displays the results obtained for test conductivity 4. Note that all three methods are smooth and without spurious artifacts. All three identify a region with low conductivity and a region with high conductivity. However, none of the methods are able to distinguish

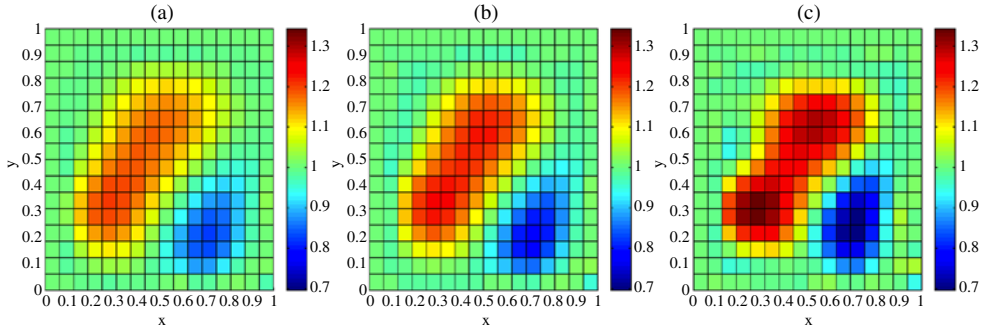

Figure 9. Reconstructions of test conductivity 4. Noise level: 1%. (a) Output least squares; (b) equation error; (c) constrained least squares.

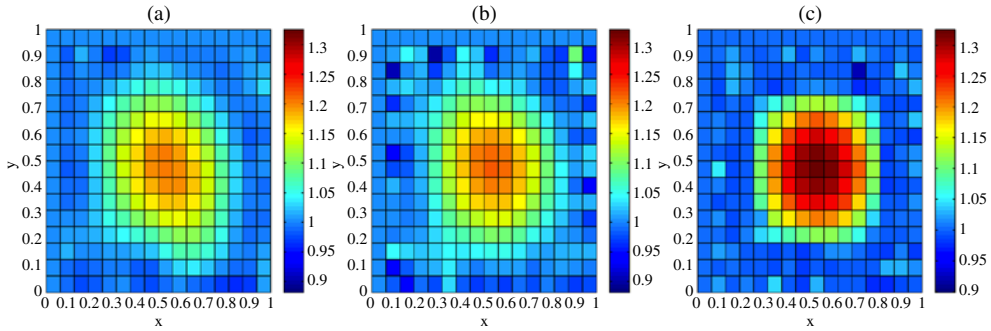

Figure 10. Reconstructions of test conductivity 1. Noise level: 3%. (a) Output least squares; (b) equation error; (c) constrained least squares.

between the two inclusions of conductivity 2. Note that both the least squares methods used the same regularization parameter, $\alpha = 10^{-5}$.

Intuitively, we can better understand why the constrained least squares methods is superior in the presence of noise by examining the iterative process of the three methods. The output least squares and equation-error methods have no explicit restrictions on σ. Thus, the iterates are allowed to move freely. We observe that they exhibit a sort of 'zig-zag' behaviour pattern and do not stay in the same feasibility region from one iteration to the next. Thus, the iterates jump in and out of the Dirichlet and Thomson feasibility regions. This behaviour can make the methods unstable, particularly in the presence of noise. In contrast, the constrained least squares method restricts the iterates to the Dirichlet infeasibility region. Hence, the constraint controls the change in σ and does not allow the 'zig-zag' behaviour to occur, and the feasibility constraint prevents the kind of instability present in the other two methods.

6.2.2. Numerical results with 3% noise. We repeat the reconstructions with data containing 3% noise and see similar results. Figures 10–13 show the reconstructed images of test conductivities 1–4 respectively. We note that, in all four tests, the three algorithms fitted the data on the boundary equally well despite the fact that the resulting images differ greatly.

In figure 11, note again that both least squares begin with the same regularization parameter, $\alpha = 10^{-3}$ which is subsequently reduced three orders of magnitude. However, the constrained least squares algorithm produces a smoother image with only one major spurious

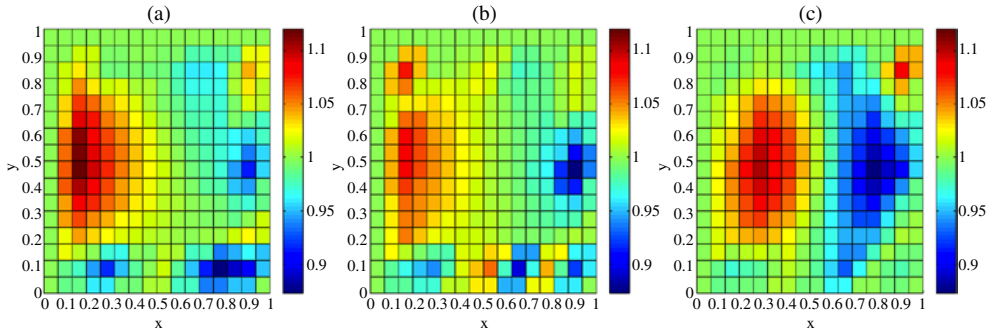

Figure 11. Reconstructions of test conductivity 2. Noise level: 3%. (a) Output least squares; (b) equation error; (c) constrained least squares.

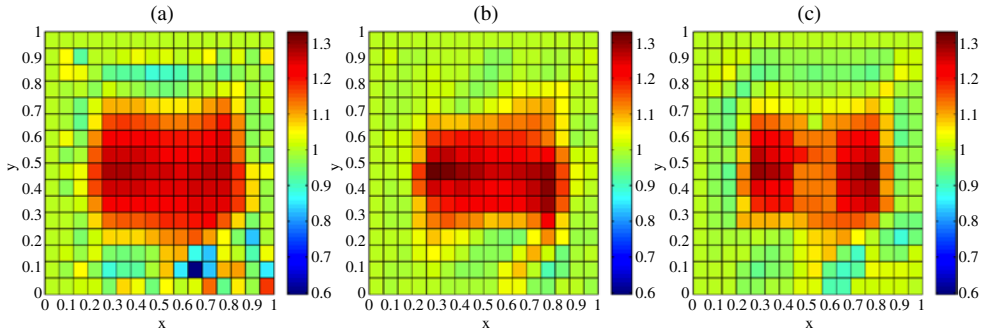

Figure 12. Reconstructions of test conductivity 3. Noise level: 3%. (a) Output least squares; (b) equation error; (c) constrained least squares.

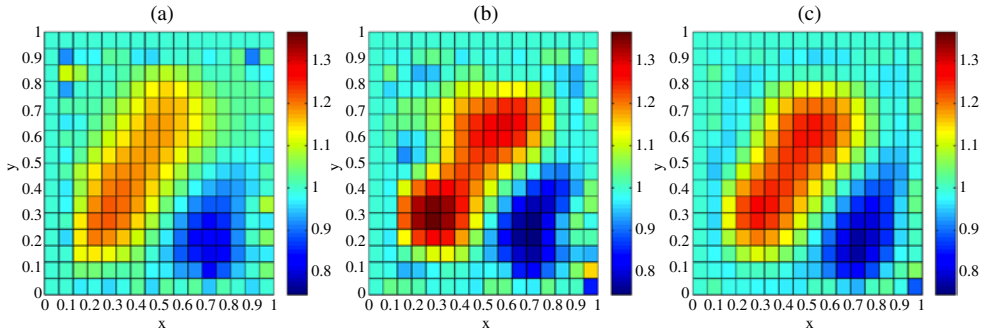

Figure 13. Reconstructions of test conductivity 4. Noise level: 3%. (a) Output least squares; (b) equation error; (c) constrained least squares.

artifact while the output least squares method includes many more artifacts and is unable to identify the region of low conductivity. The reconstructions of test conductivity 3, figure 12, show that the output least squares algorithm again produces many spurious artifacts and has no success in distinguishing between the two separate inclusions. Both variational methods produce smoother images and the constrained least squares method is able to make some distinction between the two inclusions. Furthermore, we note that the output least squares

method took approximately 2 min to run while the constrained least squares method took just under $3\frac{1}{2}$ min.

6.3. Summary of the numerical results

Based on the presented numerical results, we make the following observations on the performance of the three methods on the set of test cases.

- The constrained least squares and equation-error variational methods are more effective than output least squares. In the presence of noise, the reconstructions obtained using the constrained least squares method are superior to those of the equation-error method.
- The output least squares method fits the boundary data in the L^2 norm as well as, or better than, the constrained least squares and equation-error methods. However, the variational methods produce better images.
- In the presence of noise and with the same regularization parameter, the constrained least squares method is often able to produce smoother images with less spurious artifacts than the output least squares.

The results given in this section provide strong evidence showing that the variational methods are superior to output least squares in the presence of noise in terms of reconstruction quality. We note that these results can be improved. For example, a better regularization scheme and/or a better method for choosing the regularization parameter α should be beneficial. Furthermore, all the methods would benefit from a better initial guess σ^0, than the constant $\sigma^0 = 1$ that we have considered here. See for example results in [18, 48] where σ^0 is estimated by a multigrid approach.

7. Summary

We have introduced a set of variationally constrained reconstruction methods for EIT. The Dirichlet and Thomson variational constraints on the conductivity function σ were previously introduced by Berryman and Kohn in [13]. In this paper, we analyse the constraints and show how to use them in inversion. We discuss a variety of algorithms for the static EIT problem and describe in detail the implementation and the performance of one of them—the constrained least squares approach. Comparisons with two well known methods, the unconstrained least squares (see for example [106]) and the equation-error [70, 105], are given. Traditionally, the unconstrained least squares approach has been the method of choice, due to its simplicity and relatively low computational cost. However, the unconstrained least squares approach does not make the best use of the measured data (i.e., boundary voltage $V = (\Lambda_{\sigma^\star})^{-1} I$) because it fits the data in the convenient $L^2(\partial\Omega)$-norm, instead of the more natural and stronger $H^{1/2}(\partial\Omega)$-norm. We have shown that variational constraints can be used efficiently to achieve a better fit and that at the reconstructed σ the current density $\mathbf{j}$, satisfying the Neumann boundary conditions $-\mathbf{j}\cdot\mathbf{n}|_{\partial\Omega} = I$, and the potential ϕ, satisfying the Dirichlet boundary conditions $\phi|_{\partial\Omega} = V$, are correctly related by Ohm's law $\mathbf{j} = -\sigma\nabla\phi$. We demonstrate that achieving such a data fit can be done with an affordable computational cost and that the resulting images of σ can have better resolution than those generated by conventional, unconstrained least squares methods. Note that this work is based on the PhD thesis of GAG. For more details, please see [48].

Acknowledgments

The authors wish to thank Pamela Williams (Sandia National Laboratories) for her invaluable help installing and operating the OPT++ software used for the numerical experiments.

The authors also thank the referees for many useful suggestions and helpful references. The work of LB was partially supported by the National Science Foundation under grant number DMS-9971209 and by the Office of Naval Research under grant N00014-02-1-0088. The work of GAG was supported by a training fellowship of the Keck Center for Computational Biology (National Library of Medicine Training grant No 1T15LM07093) and by the Mathematical, Information, and Computational Sciences Program of the US Department of Energy, under contract DE-AC04-94AL85000 with Sandia Corporation. The work of YZ was partially supported by DOE grant DE-FG03-97ER25331, DOE/LANL contract 03891-99-23 and NSF grant DMS-9973339.

References

[1] Barceló J A, Barceló T and Ruiz A 2001 Stability of the inverse conductivity problem in the plane for less regular conductivities *J. Diff. Eqns* **173** 231–70

[2] Adams R A 1975 *Sobolev Spaces* (New York: Academic)

[3] Akbarzadeh M R, Tompkins W J and Webster J G 1990 Multichannel impedance pneumography for apnea monitoring *Proc. Annu. Int. Conf. IEEE Eng. Med. Biol. Soc.* **12** 1048–9

[4] Alessandrini G, Beretta E, Santosa F and Vessella S 1995 Stability in crack determination from electrostatic measurements at the boundary—a numerical investigation *Inverse Problems* **11** L17–24

[5] Alessandrini G and Rondi L 1998 Stable determination of a crack in a planar inhomogeneous conductor *SIAM J. Math. Anal.* **30** 326–40

[6] Alessandrini G 1988 Stable determination of conductivity by boundary measurements *Appl. Anal.* **27** 153–72

[7] Allers A and Santosa F 1991 Stability and resolution analysis of a linearized problem in electrical impedance tomography *Inverse Problems* **7** 515–33

[8] Arioli M, Demmel J W and Duff I S 1989 Solving sparse linear systems with sparse backward error *SIAM J. Matrix Anal. Appl.* **10** 165–90

[9] Ascher U M and Haber E 2001 Grid refinement and scaling for distributed parameter estimation problems *Inverse Problems* **17** 571–90

[10] Barber D C and Brown B H 1990 Progress in electrical impedance tomography *Inverse Problems in Partial Differential Equations* ed R Ewing, W Rundell and D L Colton (Philadelphia, PA: SIAM)

[11] Barber D and Brown B 1984 Applied potential tomography *J. Phys. E: Sci. Instrum.* **17** 723–33

[12] Berenstein C A and Casadio Tarabusi E 1996 Integral geometry in hyperbolic spaces and electrical impedance tomography *SIAM J. Appl. Math.* **56** 755–64

[13] Berryman J G and Kohn R V 1990 Variational constraints for electrical impedance tomography *Phys. Rev. Lett.* **65** 325–8

[14] Berryman J G 1990 Stable iterative reconstruction algorithm for nonlinear traveltime tomography *Inverse Problems* **6** 21–42

[15] Berryman J G 1991 Convexity properties of inverse problems with variational constraints *J. Franklin Inst.* **328** 1–13

[16] Berryman J G 1992 *Lecture Notes on Nonlinear Inversion and Tomography: II. Electrical Impedance Tomography* (presented at University of California—Berkeley)

[17] Borcea L, Berryman J G and Papanicolaou G C 1999 Matching pursuit for imaging high contrast conductive media *Inverse Problems* **15** 811–49

[18] Borcea L 2001 Nonlinear multigrid for imaging electrical conductivity and permittivity at low frequency *Inverse Problems* **17** 329–59

[19] Borcea L 2002 Electrical impedance tomography *Inverse Problems* **18** R99–136

[20] Brown R M and Uhlmann G 1997 Uniqueness in the inverse conductivity problem for nonsmooth conductivities in two dimensions *Commun. Partial Diff. Eqns* **22** 1009–27

[21] Brühl M and Hanke M 2000 Numerical implementation of two noniterative methods for locating inclusions by impedance tomography *Inverse Problems* **16** 1029–42

[22] Brühl M 2001 Explicit characterization of inclusions in electrical impedance tomography *SIAM. J. Math. Anal.* **32** 1327–41

[23] Calderón A P 1980 On an inverse boundary value problem *Seminar on Numerical Analysis and its Applications to Continuum Physics* (Rio de Janeiro: Soc. Brasileira de Matèmatica) pp 65–73

[24] Cedio-Fengya D J, Moskow S and Vogelius M S 1998 Identification of conductivity imperfections of small diameter by boundary measurements, continuous dependence and computational reconstruction *Inverse Problems* **14** 553–95

[25] Chavent G and Kunisch K 1993 Regularization in state space *J. Numer. Anal.* **27** 535–64
[26] Cheney M, Isaacson D and Newell J C 1999 Electrical impedance tomography *SIAM Rev.* **41** 85–101
[27] Cheney M and Isaacson D 1992 Distinguishability in impedance imaging *IEEE Trans. Biomed. Eng.* **39** 852–60
[28] Courant R and Hilbert D 1953 *Methods of Mathematical Physics* vol 1 (New York: Wiley)
[29] Demmel J W, Eisenstat S C, Gilbert J R, Li X S and Liu J W H 1999 A supernodal approach to sparse partial pivoting *SIAM J. Matrix Anal. Appl.* **20** 720–55
[30] Dennis J E and Schnabel R B 1996 *Numerical Methods for Unconstrained Optimization and Nonlinear Equations* (Philadelphia, PA: SIAM)
[31] Dobson D C and Santosa F 1994 Resolution and stability analysis of an inverse problem in electrical impedance tomography: dependence on the input current patterns *SIAM J. Appl. Math.* **54** 1542–60
[32] Dobson D C 1990 Stability and regularity of an inverse elliptic boundary value problem *PhD Thesis* Rice University
[33] Dobson D C 1992 Convergence of a reconstruction method for the inverse conductivity problem *SIAM J. Appl. Math.* **52** 442–58
[34] Dobson D C 1992 Estimates on resolution and stabilization for the linearized inverse conductivity problem *Inverse Problems* **8** 71–81
[35] Druskin V 1982 The unique solution of the inverse problem of electrical surveying and electrical well-logging for piecewise-continuous conductivity *Earth Phys.* **18** 51–3
[36] Druskin V 1985 On uniqueness of the determination of the three-dimensional underground structures from surface measurements with variously positioned steady-state or monochromatic field sources *Sov. Phys.—Solid Earth (Engl. transl. by American Geophysical Union)* **21** 210–4
[37] Eggleston M R, Schwabe R J, Isaacson D and Coffin L F 1989 *The Application of Electric Current Computed Tomography to Defect Imaging in Metals. Review of Progress in Quantitative NDE* ed D O Thompson and D E Chimenti (New York: Plenum)
[38] Ekeland I and Témam R 1999 *Convex Analysis and Variational Problems* (Philadelphia, PA: SIAM)
[39] Engl H W, Hanke M and Neubauer A 1996 *Regularization of Inverse Problems* (Dordrecht: Kluwer)
[40] Engl H W, Kunisch K and Neubauer A 1989 Convergence rates for Tikhonov regularization of nonlinear ill-posed problems *Inverse Problems* **5** 523–40
[41] Engl H W 1993 Regularization methods for the stable solution of inverse problems *Surv. Math. Ind.* **3** 71–143
[42] Fadeev L D 1996 Increasing solutions of the Schrödinger equation *Sov. Phys.—Dokl.* **10** 1003–35
[43] Folland G B 1995 *Introduction to Partial Differential Equations* (Princeton, NJ: Princeton University Press)
[44] Colli Franzone P, Guerri L, Taccardi B and Viganotti C 1979 *The Direct and Inverse Potential Problems in Electrocardiology. Numerical Aspects of Some Regularization Methods and Application to Data Collected in Isolated Dog Heart Experiments* (Pavia: Laboratorio di Analisi Numerica del Consiglio Nazionale delle Richerche) Pub. 222
[45] Friedman A and Vogelius M 1989 Determining cracks by boundary measurements *Indiana Univ. Math. J.* **3** 527–56
[46] Gisser D G, Isaacson D and Newell J C 1990 Electric current computed tomography and eigenvalues *SIAM J. Appl. Math.* **50** 1623–4
[47] Golub G H and Van Loan C F 1996 *Matrix Computations* 3rd edn (Baltimore, MD: Johns Hopkins University Press)
[48] Gray G A 2002 A variationally constrained numerical solution of the electrical impedance tomography problem *PhD Thesis* Rice University Technical Report 02-02
[49] Haber E, Ascher U M and Oldenburg D 2000 On optimization techniques for solving nonlinear inverse problems *Inverse Problems* **16** 1263–80
[50] Haber E and Ascher U M 2001 Preconditioned all-at-once methods for large, sparse parameter estimation problems *Inverse Problems* **17** 1847–64
[51] Hanke M 1997 Regularizing properties of a truncated Newton-CG algorithm for nonlinear inverse problems *Numer. Funct. Anal. Optim.* **18** 971–93
[52] Harris N D, Suggett A J, Barber D C and Brown B H 1987 Applications of applied potential tomography (ap) in respiratory medicine *Clin. Phys. Physiol. Meas.* A **8** 155–65
[53] Hofmann B 1998 Approximation of the inverse electrical impedance tomography problem by an inverse transmission problem *Inverse Problems* **14** 1171–87
[54] Holder D 1993 *Clinical and Physiological Applications of Electrical Impedance Tomography* (London: UCL Press)
[55] Hough P, Meza J and Williams P *OPT++: an Object-Oriented Nonlinear Optimization Library* http://csmr.ca.sandia.gov/projects/opt++/

[56] Ikehata M and Siltanen S 2000 Numerical method for finding the convex hull of an inclusion in conductivity from boundary measurements *Inverse Problems* **16** 1043–52
[57] Ikehata M 1998 Reconstruction of an obstacle from the scattering amplitude at a fixed frequency *Inverse Problems* **14** 949–54
[58] Ikehata M 1998 Reconstruction of the shape of the inclusion by boundary measurements *Commun. Part. Diff. Eqns* **23** 1459–74
[59] Ikehata M 2000 Reconstruction of the support function for inclusion from boundary measurements *J. Inverse Ill-Posed Problems* **8** 367–78
[60] Isaacson D and Cheney M 1990 Current problems in impedance imaging *Inverse Problems in Partial Differential Equations* ed D Colton, R Ewing and W Rundell (Philadelphia, PA: SIAM) pp 141–9
[61] Isaacson D 1986 Distinguishabiltiy of conductivities by electric current computed tomography *IEEE Trans. Biomed. Eng.* **5** 91–5
[62] Isakov V 1998 *Inverse Problems for Partial Differential Equations* (New York: Springer)
[63] Jackson J D 1974 *Classical Electrodynamics* 2nd edn (New York: Wiley)
[64] Jikov V V, Kozlov S M and Oleinik O A 1991 *Homogenization of Differential Operators and Integral Functionals* (Berlin: Springer)
[65] Johnson C 2002 Inverse bioelectric field problems: modeling, simulation, and visualization *Invited Lecture at the SFB-Conf. on Computational Methods for Inverse Problems (Strobl, Austria, Aug. 2002)*
[66] Kaipio J P, Kolehmainen V, Somersalo E and Vauhkonen M 2000 Statistical inversion and Monte Carlo sampling methods in electrical impedance tomography *Inverse Problems* **16** 1487–522
[67] Kaipio J P, Kolehmainen V, Vauhkonen M and Somersalo E 1999 Inverse problems with structural prior information *Inverse Problems* **15** 713–29
[68] Kaltenbacher B 2001 On the regularizing properties of a full multigrid method for ill-posed problems *Inverse Problems* **17** 767–88
[69] Keller G V 1988 *Electrical Properties of Rocks and Minerals, Handbook of Physical Constants* ed S P Clarck Jr (New York: Geological Society of America) pp 553–77
[70] Kohn R V and McKenney A 1990 Numerical implementation of a variational method for electrical impedance tomography *Inverse Problems* **6** 389–414
[71] Kohn R V and Vogelius M 1984 Determining conductivity by boundary measurements *Commun. Pure Appl. Math.* **37** 113–23
[72] Kohn R V and Vogelius M 1985 Determining conductivity by boundary measurements II. Interior results *Commun. Pure Appl. Math.* **38** 643–67
[73] Kohn R V and Vogelius M 1987 Relaxation of a variational method for impedance computed tomography *Commun. Pure Appl. Math.* **40** 745–77
[74] Kunisch K and Zou J 1998 Iterative choices of regularization parameters in linear inverse problems *Inverse Problems* **14** 1247–64
[75] Luo S, Afonso V X, Webster J G and Tompkins W J 1992 The electrode system in impedance-based ventilation measurements *IEEE Trans. Biomed. Eng.* **39** 1130–41
[76] Mandache N 2001 Exponential instability in an inverse problem for the Schrödinger equation *Inverse Problems* **17** 1435–44
[77] Morozov V A 1966 On the solution of functional equations by the method of regularization *Doklady* **167** 414–7
[78] Morozov V A 1984 *Methods for Solving Incorrectly Posed Problems* (Berlin: Springer)
[79] Nachman A I 1996 Global uniqueness for a two-dimensional inverse boundary problem *Ann. Math.* **143** 71–96
[80] Nocedal J and Wright S J 1999 *Numerical Optimization* (*Springer Series in Operations Research*) (New York: Springer)
[81] Novikov R G and Khenkin G M 1987 The $\bar{\partial}$-equation in the multidimensional inverse scattering problem *Usp. Mat. Nauk* **42** 93–152
[82] Novikov R G 1988 Multidimensional inverse spectral problem for the equation $-\delta\psi + (v(x) - eu(x))\psi = 0$ *Funct. Anal. Appl.* **22** 263–72
[83] O'Sullivan F 1986 A statistical perspective on ill-posed inverse problems *Stat. Sci.* **1** 502–27
[84] Päivärinta L, Panchencko A and Uhlmann G 2003 Complex geometrical optics solutions for Lipschitz conductivities *Rev. Mat. Iberoam.* **19** 57–72
[85] Parker R L 1984 The inverse problem of resistivity sounding *Geophysics* **142** 2143–58
[86] Parker R L 1994 *Geophysical Inverse Theory* (Princeton, NJ: Princeton University Press)
[87] Ramirez A, Daily W, Binley A, LaBrecque D and Roelant D 1996 Detection of leaks in underground storage tanks using electrical resistance methods *J. Env. Eng. Geophys.* **1** 189–203

[88] Ramirez A, Daily W, LaBrecque D, Owen E and Chestnut D 1993 Monitoring an underground steam injection process using electrical resistance tomography *Water Resources Res.* **29** 73–87
[89] Santosa F, Kaup P and Vogelius M 1996 A method for imaging corrosion damage in thin plates from electrostatic data *Inverse Problems* **12** 279–93
[90] Santosa F and Vogelius M 1990 A backprojection algorithm for electrical impedance imaging *SIAM J. Appl. Math.* **50** 216–43
[91] Santosa F and Vogelius M 1991 A computational algorithm for determining cracks from electrostatic boundary measurements *Int. J. Eng. Sci.* **29** 917–38
[92] Schwan H P and Kay C F 1957 The conductivity of living tissues *Ann. NY Acad. Sci.* **65** 1007–13
[93] Seagar A 1983 Probing with low frequency electric currents *PhD Thesis* University of Canterbury
[94] Seppänen A, Vauhkonen M, Vauhkonen P J, Somersalo E and Kaipio J 2001 State estimation with fluid dynamical evolution models in process tomography—an application to impedance tomography *Inverse Problems* **17** 467–84
[95] Siltanen S, Mueller J and Isaacson D 2000 An implementation of the reconstruction algorithm of A. Nachman for the 2D inverse conductivity problem *Inverse Problems* **16** 681–99
[96] Somersalo E, Cheney M and Isaacson D 1992 Existence and uniqueness for electrode models for electric current computed tomography *SIAM J. Appl. Math.* **52** 1023–40
[97] Sylvester J and Uhlmann G 1987 A global uniqueness theorem for an inverse boundary value problem *Ann. Math.* **125** 153–69
[98] Sylvester J and Uhlmann G 1990 The Dirichlet to Neumann map and applications *Inverse Problems in Partial Differential Equations* ed R Ewing, W Rundell and D L Colton (Philadelphia, PA: SIAM)
[99] Tamburrino A and Rubinacci G 2002 A new non-iterative inversion method for electrical resistance tomography *Inverse Problems* **18** 1809–29
[100] Tikhonov A N and Arsenin V Y 1977 *Solutions of Ill-Posed Problems,* transl. ed F John (Washington, DC: Wiley)
[101] Tikhonov A N, Leonov A S and Yagola A G 1998 *Nonlinear Ill-Posed Problems, Applied Mathematics and Mathematical Computation* vols 1 and 2 (London: Chapman and Hall) Engl. lang. edn
[102] Uhlmann G 1999 Developments in inverse problems since Calderón's foundational paper *Harmonic Analysis and Partial Differential Equations (Chicago Lectures in Math)* (Chicago, IL: University of Chicago Press) pp 295–345
[103] Vauhkonen P J, Vauhkonen M and Kaipio J 2001 Fixed-lag smoothing and state estimation in dynamic electrical impedance tomography *Int. J. Numer. Methods Eng.* **50** 2195–209
[104] Vauhkonen P J, Vauhkonen M, Savolainen T and Kaipio J 1999 Three-dimensional electrical impedance tomography based on the complete electrode model *IEEE Trans. Med. Eng.* **46** 1150–60
[105] Wexler A, Fry B and Neuman M 1985 Impedance-computed tomography algorithm and system *Appl. Opt.* **24** 3985–92
[106] Yorkey T J, Webster J G and Tompkins W J 1987 Comparing reconstruction algorithms for electrical impedance tomography *IEEE Trans. Biomed. Eng.* **34** 843–52